Data-Driven Planning for Wireless Charging Lanes

Canqi Yao, Jianqiang Cheng, *Member, IEEE*, Kai Pan, *Member, IEEE*

***Abstract*—The widespread adoption of electric vehicles (EVs) is significantly hindered by the long charging time and range anxiety resulting from slow charging speed and limited battery capacity. Meanwhile, wireless charging lanes (WCLs) and solar-powered EVs (SEVs) offer a promising solution by providing wireless and solar charging power while driving. Under this circumstance, addressing the optimal planning of WCLs while considering SEV operations is crucial for facilitating the widespread adoption of EVs. Considering the uncertain solar power harvesting of SEVs, we propose a data-driven two-stage distributionally robust optimization (DRO) model for this integrated planning and operation problem. In the first stage, we optimize the deployment of WCLs with budget constraints, and the second stage determines the optimal operation schedules of SEVs under uncertain solar charging power characterized by a moment-based ambiguity set. To address the computational challenges (due to the discrete variables in both stages and the infinite-dimensional optimization in the second stage), we develop two approximation models and an integrated distributed method. Finally, extensive numerical experiments with synthetic and real transportation networks are conducted to demonstrate the effectiveness and scalability of our proposed models and algorithms. Specifically, the proposed DRO model achieves a 1.17% lower total cost in out-of-sample tests than the sample average approximation method, and with higher wireless charging power rates and increased battery capacities, we can build fewer WCLs.**

***Index Terms*—Integrated planning and operation problem, wireless charging lanes, solar-powered electric vehicles, two-stage distributionally robust optimization.**

NOMENCLATURE

Indices and Sets

$\boldsymbol{P}_d$	Set of partitioned support in period d
$\mathcal{D}, \mathcal{K}, \mathcal{V}, \mathcal{E}$	Set of all periods, all SEVs, all nodes, and all roads
$\mathcal{Z}$	Set of planning variables of WCLs
$d, k, i, (i,j)$	Index of time periods, SEVs, nodes and roads
F_d, S_d	Set of dual variables of the second-stage problem in period d, the support set of the uncertain solar charging power in period d

Parameters

η^{w}_{ijd}	Wireless charging coefficient of the WCL (i,j) in period d
α_z	Step size of the subgradient method
$\bar{C}_i$	Construction budget of the WCLs for i, [\$]
$\bar{E}_k$	Battery capacity of SEV k, [kW h]
$\bar{P}_{ij}$	Rated wireless charging power of road (i,j), [kW]
$\boldsymbol{\mu}_d$	The mean of uncertain solar charging power in period d, $\boldsymbol{\mu}_d = (\mu_{ijd}, \forall (i,j) \in \mathcal{E})^\top$
$\underline{\boldsymbol{x}}^{\mathrm{c}}_d, \bar{\boldsymbol{x}}^{\mathrm{c}}_d$	Lower and upper bounds of continuous variables in period d
$\boldsymbol{b}^{\mathrm{e}}, \boldsymbol{b}^{\mathrm{i}}, \boldsymbol{h}^{\mathrm{e}}, \boldsymbol{h}^{1}$	Right-hand-side constant vectors of constraints in the second-stage problem
$\boldsymbol{c}$	Construction cost vector of the WCLs, [\$]
$\boldsymbol{q}^{\mathrm{b}}, \boldsymbol{q}^{\mathrm{c}}$	Objective coefficient vector of binary and continuous variables
$\omega_{\mathrm{T}}, \omega_{\mathrm{E}}$	Value of time and energy, [\$/h, \$/kW]
ϕ_d	Energy consumption rate of SEVs in period d, [kW h/km]
Σ_d	The variance of uncertain solar charging power in period d, $\Sigma_d = diag(\sigma^2_{ijd}, \forall (i,j) \in \mathcal{E})$
$\underline{C}$	Penetration rate of the WCLs
A^{e} / W^{ce}	Coefficient matrix for binary/continuous variables in equality constraints
A^{i}	Coefficient matrix for binary variables in inequality constraints
$B_{dp}, \boldsymbol{b}_{dp}$	Coefficient matrix and constant vector of the hyperplanes in partitioned support p and period d
c^{v}	Usage cost of an SEV, [\$]
D_i	Negative value of the delivery revenue at customer node i, [\$]
d_{ij}, e_{ijd}	Travel distance of road (i,j), energy consumption of road (i,j) in period d, [km, kW h/km]
E_{0kd}	Initial battery level of SEV k in period d, [kW h]
H^2, H^3	Constraint coefficient matrix of the random vector and first-stage variables
L	Lower bound of the second-stage problem
M	A sufficiently large constant for the linearization of bilinear terms
p_{ijd}	Wireless charging price of road (i,j) in period d, [\$]
T_{ijd}	Travel time of road (i,j) in period d, [h]
$t^{\mathrm{L}}_{jd}, t^{\mathrm{U}}_{jd}$	Time window of customer i in period d, [h]
W^{b} / W^{c}	Coefficient matrix for binary/continuous variables in inequality constraints

Random Variables

$\boldsymbol{\xi}_d$	Solar charging power in period d, $\boldsymbol{\xi_d} = (\xi_{ijd}, \forall (i,j) \in \mathcal{E})^\top$, [kW]

Decision Variables

$\boldsymbol{v}_{dp}$	Continuous decision vector of partition p in period d
$\boldsymbol{\beta}_d$	Continuous dual variables in period d corre-

Canqi Yao and Kai Pan are with the Department of Logistics and Maritime Studies, The Hong Kong Polytechnic University, Hong Kong. Jianqiang Cheng is with the Department of Systems and Industrial Engineering, University of Arizona, Tucson, AZ, USA. Emails: canqi.yao@polyu.edu.hk (CY), jqcheng@email.arizona.edu (JC), kai.pan@polyu.edu.hk (KP). Kai Pan was supported in part by the Research Grants Council of Hong Kong [Grant 15503723]. Jianqiang Cheng is supported in part by the National Science Foundation [Grants ECCS-2143679 and 2404412]. *(Corresponding author: Kai Pan).*

sponding to the support, mean, and variance information of $\mathcal{P}_d$, $\boldsymbol{\beta}_d = \{\gamma_d, \boldsymbol{\alpha}_d, \boldsymbol{Q}_d\}$

$\boldsymbol{\lambda}_d$ Continuous dual variables of the second-stage problem in period d, $\boldsymbol{\lambda}_d = \{\boldsymbol{\lambda}_d^{\mathrm{be}}, \boldsymbol{\lambda}_d^{\mathrm{bi}}, \boldsymbol{\lambda}_d^{\mathrm{ce}}, \boldsymbol{\lambda}_d^{\mathrm{ci}}\}$

$\boldsymbol{\pi}_d$ Continuous dual variables for the constraint $\boldsymbol{y}_d = \boldsymbol{z}^*$ in period d

$\boldsymbol{\zeta}_{dp}$ Continuous dual variables of partition p in period d, $\boldsymbol{\zeta}_{dp} = \{\zeta_{dp}^{\mathrm{s1}}, \zeta_{dp}^{\mathrm{s2}}, \zeta_{dp}^{\mathrm{c1}}, \zeta_{dp}^{\mathrm{c2}}, \zeta_{dp}^{\mathrm{l1}}, \zeta_{dp}^{\mathrm{l2}}, \zeta_{dp}^{\mathrm{u1}}, \zeta_{dp}^{\mathrm{u2}}\}$

$\boldsymbol{\zeta}_d$ Continuous dual variables of the support set S_d in period d

$\boldsymbol{s}_{dp}$ Continuous auxiliary variable vector of partition p in period d

$\boldsymbol{s}_{dv}$ Continuous auxiliary variable vector for the decomposition of PSD matrix in period d and extreme point v

$\boldsymbol{S}_d$ Continuous slack variables for the constraint of the second-stage problem in period d

$\boldsymbol{x}_{dp}^{\mathrm{b}}/\boldsymbol{x}_{dp}^{\mathrm{c}}$ Local copy of the binary/continuous variables of partition p in period d

$\boldsymbol{x}_d^{\mathrm{b}}/\boldsymbol{x}_d^{\mathrm{c}}$ All binary/continuous variables of the second-stage problem in period d

$\boldsymbol{y}_d$ Local copy of the continuous variables for $\boldsymbol{z}$ in period d

$\mathscr{A}_{dp}^{\mathrm{c}}$ Continuous decision matrix of partition p in period d

θ Continuous auxiliary variable for the epigraph formulation of the second-stage problem

$E_{ijd}^{\mathrm{s}}/E_{ijd}^{\mathrm{u}}$ Continuous variables indicating the used/unused solar energy at road (i,j) in period d, [kW h]

E_{ijd}^{w} Continuous variables indicating the charged wireless energy at road (i,j) in period d, [kW h]

E_{ikd} Continuous variables indicating the battery level of SEV k at node i in period d, [kW h]

$f_{ijkd}^{\mathrm{z}}, f_{ijkd}^{\mathrm{x}}$ Continuous auxiliary variables for the linearization of trilinear terms

t_{jkd} Continuous variables indicating the arrival time of SEV k at node j in period d, [h]

x_{ijkd} Binary variables indicating whether SEV k traverses road (i,j) in period d

z_{ij} Binary variables indicating whether a WCL is installed at road (i,j)

Acronyms

DA Distributed algorithm
DCG Delayed constraint generation
DRO Distributionally robust optimization
EVs Electric vehicles
IWS Integrated WCL planning and SEV operations
LB Lower bound
LDR Linear decision rule
LP Linear program
MILP Mixed integer linear program
MISOCP Mixed integer second-order cone program
PSD Positive semi-definite
SDP Semidefinite program
SEVs Solar-powered electric vehicles
SOCP Second-order cone programming
UB Upper bound
WCLs Wireless charging lanes

I. Introduction

To achieve carbon neutrality, an increasing number of countries promote the adoption of EVs [1]. However, a few setbacks, e.g., *charging time and range anxiety* [2]–[7], hinder the widespread adoption of EVs. To circumvent the *charging time anxiety*, WCLs providing in-motion wireless charging service [8] serve as effective alternatives for energy replenishment. In 2023, the first wireless charging road in the US was deployed in Detroit, allowing electric buses or trucks to wirelessly charge with up to $100\,\mathrm{kW}$ while driving [9]. In addition, SEVs, another option promoting the widespread adoption of EVs, can mitigate the *range anxiety* for the supplementary mileage provided by solar energy [10]. Hence, WCLs and SEVs complement the limited range of EVs, making them good fits to support the widespread adoption of electrified mobility.

It is worth noting that the operational decisions of SEVs heavily depend on the planning schedules of WCLs (see Fig. 1 for the illustration of such dependence). Specifically, SEVs traveling on WCLs benefit from two energy sources: wireless and solar power. Without WCLs, SEVs rely exclusively on solar power, which is highly unpredictable, to recharge their batteries. Thus, we aim to address the following question in this paper: *How can we jointly make decisions regarding the WCL planning and SEV operations under uncertainty?* To that end, this paper investigates the planning of WCLs with the optimal operation of SEVs under uncertain solar charging power. The integration of WCLs and SEVs offers a promising solution to overcome the limitations of EVs by ensuring continuous charging service availability and reducing dependency on stationary charging stations. These emerging technologies ultimately contribute to enhancing the adoption rate of EVs to achieve sustainable transportation.

A. Related Literature

Planning of WCLs. With the development of wireless power transfer technology [11], an increasing number of works investigate the planning of WCLs (see, e.g., [12]–[16]), which play a crucial role in facilitating the integration of massive EVs into existing transportation systems. For example, to study the adverse effects of wireless charging on road capacity, [14] provides a bi-level optimization model in which the upper level determines the location of WCLs and the lower level models the user equilibrium of electric traffic assignment. However, range anxiety, a crucial limitation of EVs, is not incorporated into the optimal deployment problem of WCLs therein.

Planning of WCLs with Range Anxiety. To address the limited battery capacity, some studies investigate an optimal configuration of WCLs considering the range anxiety of EVs (see, e.g., [17]–[22]). For example, to capture the interaction between the distribution company and EV operator, [17] presents a bi-level planning model to deploy the WCLs considering the state-of-charge constraints. Similarly, [19] presents a bi-level planning model for wireless charging systems incorporating

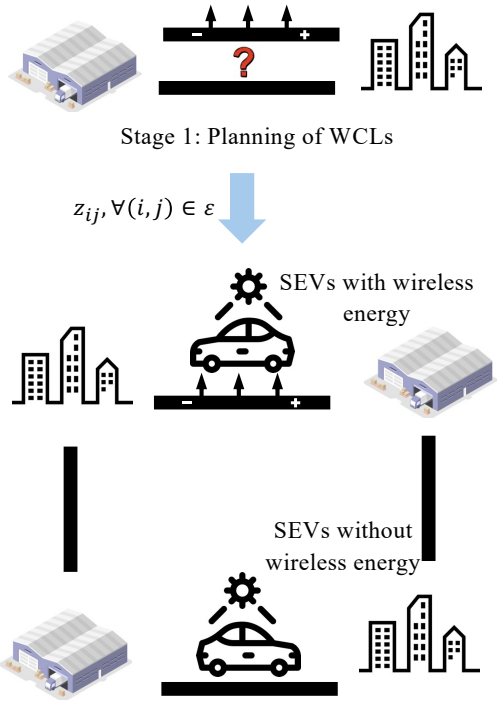

Fig. 1: Integrated WCL Planning and SEV Operations.

the charging requirement and range anxiety of EVs. Driven by the trade-off between the costs of deploying wireless charging infrastructure and manufacturing batteries, [22] proposes an integrated wireless charging facilities deployment model for the general transport networks. However, these papers fail to capture uncertain parameters (e.g., charging power) for the optimal planning problem of wireless charging systems.

Planning of WCLs with Uncertainties. On a strategic level, the charging facility location problem and the electric fleet operation problem should be considered simultaneously to derive optimal solutions [23]. Nevertheless, significant uncertainties are involved in such an integrated planning and operation problem of energy and transportation systems [24] and cannot be ignored for the optimal planning of wireless charging systems. To handle the uncertainties in energy consumption and travel time, [25] presents a robust planning model of wireless charging infrastructures. Following [25], to optimize the battery capacity, the location and number of transmitters, and the number of inverters and battery electric buses, [26] provides a more complicated robust optimization model for wireless charging systems. To determine the wireless charging facility deployment, battery size, and wireless charging schedule simultaneously, [27] proposes a two-stage robust model to handle the energy consumption and travel time uncertainty.

Operation of SEVs. The optimal deployment of WCLs resolves the issue of long charging time by providing in-motion charging services, potentially promoting the widespread adoption of EVs. Meanwhile, the additional mileage from the solar energy of SEVs can also reduce reliance on grid electricity and partially resolve the range anxiety of EVs. However, limited papers work on the optimal operation problem of SEVs (see, e.g., [10], [28], [29]). Due to the unpredictable solar availability, [28] proposes a route planning model for SEVs to balance electricity harvesting and consumption incorporating time constraints. To study the planning and operation of SEVs, [29] solves the charging station placement, charging assignment, and route planning problems sequentially, which ignores solar power uncertainty and fails to obtain a global optimal solution for the proposed sequential solution method.

In Table I, we classify the reviewed papers based on their focus areas, including WCLs, SEVs, range anxiety, uncertainty, DRO, decomposition method, the 2nd-stage model, and solution method. Although a few papers have investigated the planning of WCLs and the operation of SEVs separately, none of them investigates the integrated WCL planning and SEV operations. Note that such integration is crucial for alleviating the range anxiety of EVs and further supporting the widespread adoption of electrified mobility. This research gap highlights the novelty and significance of our study in addressing the emerging integrated planning of WCLs and SEVs. As summarized in Table I, to the best of our knowledge, we are the first to investigate the planning problem of WCLs while considering the operation of SEVs and uncertain solar charging power. Specifically, we propose a two-stage data-driven distributionally robust optimization model with a moment-based ambiguity set for this integrated planning and operation problem. We optimize the planning of WCLs in the first stage and formulate the operation problem of SEVs with solar power uncertainty as a mixed integer linear program (MILP) in the second stage. Such a problem is significantly challenging because of the discrete variables in both stages and the infinite-dimensional optimization in the second stage. To address the challenge, we develop a reformulation approach consisting of linear programming (LP) relaxation, semidefinite program (SDP) reformulation, and second-order cone programming (SOCP) reformulation to obtain an outer approximation model. We solve this model via a delayed constraint generation (DCG) algorithm, obtaining an efficient lower bound (LB) of the original problem. To quantify the solution quality by the DCG method, we propose a linear decision rule (LDR) based inner approximation model, which allows a distributed implementation with a given planning decision of WCLs, obtaining an efficient upper bound (UB) of the original problem. To further improve the quality of LB, we develop integer optimality, subgradient, and feasibility cuts to strengthen our outer approximation model.

B. Contribution

Our paper's contribution can be summarized as follows.

- To the best of our knowledge and according to our literature review in Table I, we are the first paper to investigate the planning problem of WCLs while considering the operation of SEVs and uncertain solar charging power. To tackle the integrated planning and operation problem, we propose a data-driven two-stage DRO model that solves the planning problem of WCLs in the first stage and the operation problem of SEVs in the second stage.
- To address the significant computational challenges: (1) discrete variables in both stages and (2) infinite-dimensional

TABLE I: Comparison with State-of-the-Art Works

Reference	WCLs	SEVs	Range anxiety	Uncertainty	DRO	Decomposition	2nd model	Solution method
[10]	✗	✓	✓	✗	✗	✗	N.A.	Solver
[11]	✓	✗	✗	✗	✗	✗	Convex	KKT
[14]	✓	✗	✗	✗	✗	✗	N.A.	Solver
[17]	✓	✗	✓	✗	✗	✗	Convex	KKT
[19]	✓	✗	✓	✗	✗	✗	N.A.	BB
[20]	✓	✗	✓	✗	✗	✗	N.A.	Solver
[21]	✓	✗	✓	✗	✗	✗	MILP	Solver
[22]	✓	✗	✓	✗	✗	✗	N.A.	SO
[24]	✓	✗	✓	✓	✗	✗	N.A.	PSO
[25]	✓	✗	✓	✓	✗	✗	SIP	AARC
[26]	✓	✗	✓	✓	✗	✗	MILP	Solver
[27]	✓	✗	✓	✓	✗	✓	Convex	C&CG
[29]	✗	✓	✓	✗	✗	✗	N.A.	DP
Our paper	✓	✓	✓	✓	✓	✓	MISOCP	DCG, LDR

* N.A.: Not available, KKT: Karush–Kuhn–Tucker conditions, C&CG: Column-and-constraint generation method, PSO: Particle swarm optimization, DP: Dynamic programming, SIP: semi-infinite programming model, AARC: affinely adjustable robust counterpart, BB: Branch and bound method, SO: Surrogate optimization method.

optimization in the second stage, we design an outer approximation model using LP relaxation and SOCP reformulation, leading to an LB for the original model. To quantify the solution quality of the LB, with a partitioned support set, LDR, and K-adaptability reformulation, we develop a mixed-integer second-order cone programming (MISOCP)-based inner approximation model, leading to a UB for the original problem.

- To further relieve the computational burden of solving the large-sized inner approximation model, we propose a DCG-based method that efficiently solves the outer approximation and inner approximation model in a distributed manner.

C. Organization

The paper unfolds as follows. We elaborate on our two-stage DRO model in Section II. Then, we propose an outer approximation model in Section III to solve the original model as an MISOCP, which can be solved efficiently by a DCG method. To quantify the solution quality by the DCG method, we design an inner approximation model in Section IV based on a partitioned support set and LDR. In Section V, an integrated solution algorithm consisting of the DCG method and three LB-improvement cuts is developed to solve the outer and inner approximation models in a distributed manner. In Section VI, extensive numerical experiments are implemented to evaluate the effectiveness of our solution approaches. We conclude this paper in Section VII.

II. Mathematical Model

In this section, anticipating an operational horizon with a set of periods $\mathcal{D}$, we describe a two-stage DRO model for Integrated WCL planning and SEV operations (IWS) under uncertain solar power. Specifically, we consider a transportation service network to serve customers in a set of locations $\mathcal{R}_d$ in each period $d \in \mathcal{D}$. Thus, given a period $d \in \mathcal{D}$, we represent the service network using a directed graph $\mathcal{G} := (\mathcal{V}, \mathcal{E})$, where (i) $\mathcal{V} = \{v_1, \mathcal{R}_d, v_n\}$ comprises a start depot v_1, an end depot v_n, and the set of customer nodes $\mathcal{R}_d$; (ii) $\mathcal{E}$ is the set of roads with $(i,j) \in \mathcal{E}$ denoting a road from nodes i to j. Note that the network $\mathcal{G}$ varies in different periods for different customers, and thus, we omit the index $d \in \mathcal{D}$ for the network $\mathcal{G}$ for brevity. We also let $\mathcal{V}_1 := \mathcal{V} \setminus \{v_1\}$ and $\mathcal{V}_n := \mathcal{V} \setminus \{v_n\}$. Anticipating the operations with a set of SEVs $\mathcal{K}$ in the coming operational horizon, we decide whether a WCL should be built along road $(i,j) \in \mathcal{E}$ (denoted by a binary variable $z_{ij} = 1$) or not (i.e., $z_{ij} = 0$).

For any $(i,j) \in \mathcal{E}$ and $d \in \mathcal{D}$, the solar charging power ξ_{ijd} is subject to variability due to changing weather conditions and solar radiation levels. Although such uncertainty is significant, historical data is available (e.g., recorded by various observatories) to help characterize the unknown distribution $\mathbb{P}_d$ of $\boldsymbol{\xi_d} = (\xi_{ijd}, \forall (i,j) \in \mathcal{E})^\top \in \mathbb{R}^{|\mathcal{E}|}$ for any $d \in \mathcal{D}$. We let $\vartheta = |\mathcal{E}|$. Thus, we collect the moment information of $\boldsymbol{\xi}_d$ for each $d \in \mathcal{D}$ from the available data and assume $\mathbb{P}_d$ runs in a distributional ambiguity set $\mathcal{P}_d$ specified by the collected moment information as follows:

$$\mathcal{P}_d\left(S_d, \boldsymbol{\mu}_d, \boldsymbol{\Sigma}_d\right) = \left\{ \mathbb{P}_d \;\middle|\; \begin{array}{l} \mathbb{P}_d\left(\boldsymbol{\xi}_d \in S_d\right) = 1 \\ \mathbb{E}_{\mathbb{P}_d}\left[\boldsymbol{\xi}_d\right] = \boldsymbol{\mu}_d \\ \mathbb{E}_{\mathbb{P}_d}\left[\left(\xi_{ijd} - \mu_{ijd}\right)^2\right] \\ \qquad \leq \sigma_{ijd}^2, \forall (i,j) \in \mathcal{E} \end{array} \right\}, \quad (1)$$

where S_d, $\boldsymbol{\mu}_d = (\mu_{ijd}, \forall (i,j) \in \mathcal{E})^\top$, and σ_{ijd}^2 represent the support set, mean, and variance of $\boldsymbol{\xi}_d$, respectively. Here, S_d is polyhedral and bounded, i.e., $S_d = \{\boldsymbol{\xi}_d | A_d \boldsymbol{\xi}_d \leq \boldsymbol{b}_d\}$ with $A_d \in \mathbb{R}^{\ell \times \vartheta}$ and $\boldsymbol{b}_d \in \mathbb{R}^\ell$, with at least one interior point.

We let $\boldsymbol{c} = (c_{ij}, \forall (i,j) \in \mathcal{E})^\top$ denote the construction cost vector of the WCLs, and $\underline{C}$ and $\bar{C}_i$ denote the penetration rate of WCLs and the construction budget for each node $i \in \mathcal{V}$, respectively. We use $\mathbb{1} \in \mathbb{R}^\vartheta$ to denote a column vector where every entry is 1. Given a WCL planning decision $\boldsymbol{z} = (z_{ij}, \forall (i,j) \in \mathcal{E})^\top$ and a realization of random solar power $\boldsymbol{\xi}_d$ in each period $d \in \mathcal{D}$, we use $U_d(\boldsymbol{z}, \boldsymbol{\xi}_d)$ to denote the coming operational cost in this period. To build a robust service network, we provide the following two-stage DRO model for the IWS problem to minimize the first-stage construction ($\boldsymbol{c}^\top \boldsymbol{z}$) and second-stage operational costs while ensuring customer services are fulfilled and uncertain solar power is harvested.

Problem 1 (Two-stage DRO model for IWS)**.**

$$\min_{\boldsymbol{z}} \quad \boldsymbol{c}^\top \boldsymbol{z} + \sum_{d\in\mathcal{D}} \max_{\mathbb{P}_d\in\mathcal{P}_d} \mathbb{E}_{\mathbb{P}_d}\left[U_d(\boldsymbol{z},\boldsymbol{\xi_d})\right]$$

$$\text{s.t.} \quad \underline{C}\vartheta \le \mathbb{1}^\top \boldsymbol{z}, \tag{2a}$$

$$\sum_{j\in\mathcal{V}} c_{ij} z_{ij} \le \bar{C}_i,\ \forall i \in \mathcal{V}, \tag{2b}$$

where (2a) specifies the minimum penetration requirement for the installed WCLs [11] and (2b) specifies the construction budget at each node [17]. We use a set $\mathcal{Z}$ to collect constraints (2). Note that the detailed description of $U_d(\boldsymbol{z},\boldsymbol{\xi}_d)$ in each period $d \in \mathcal{D}$ depends on how we operate the SEV fleet in the second stage, as detailed below.

Specifically, given $\boldsymbol{z}$ and $\boldsymbol{\xi}_d$ ($\forall d \in \mathcal{D}$), we consider a multi-period SEV operation model over the corresponding service network $\mathcal{G}$ in the second stage. For any $d \in \mathcal{D}$, we define the following notations. (i) For any $i, j \in \mathcal{V}$, we use d_{ij} to denote the travel distance of road (i, j) and T_{ijd} and e_{ijd} to denote the travel time and energy consumption of road (i, j) in period d, respectively. (ii) For any $i \in \mathcal{V}$ and $k \in \mathcal{K}$, we denote the arrival time and battery level of SEV k at the customer i in period d by t_{ikd} and E_{ikd}, respectively. (iii) For any $i, j \in \mathcal{V}$ and $k \in \mathcal{K}$, we use a binary variable x_{ijkd} to indicate whether SEV k traverses road (i, j) in period d. Given each period $d \in \mathcal{D}$, we present the second-stage model with detailed constraints provided below.

1) Routing-related Constraints: First, an SEV entering a customer node has to leave the same customer node, and SEVs starting at the start depot return to the end depot after serving the customers. Thus, we can formulate the vehicle flow conservation constraints [30] as

$$\sum_{j\in\mathcal{V}} x_{ijkd} - \sum_{j\in\mathcal{V}} x_{jikd} = \varrho_i, \quad \forall i \in \mathcal{V}, k \in \mathcal{K}, \tag{3a}$$

$$\varrho_i = \begin{cases} 1, -1, & \text{if } i \in \{v_1, v_n\}, \text{ respectively,} \\ 0, & \text{otherwise.} \end{cases} \tag{3b}$$

Second, each customer can be served at most once by the SEV fleet, as shown below.

$$\sum_{k\in\mathcal{K}} \sum_{j\in\mathcal{V}} x_{ijkd} \le 1, \quad \forall i \in \mathcal{R}_d, \tag{4}$$

Third, we denote the time window of customer j in period d as $(t^{\mathrm{L}}_{jd}, t^{\mathrm{U}}_{jd})$. Each customer should be served during their time windows, as shown below.

$$t^{\mathrm{L}}_{jd} \le t_{jkd} \le t^{\mathrm{U}}_{jd}, \quad \forall j \in \mathcal{R}_d, \tag{5}$$

Meanwhile, the visiting time of SEVs should satisfy the following constraints

$$\begin{aligned} t_{jkd} \ge & T_{ijd} + t_{ikd} - M(1 - x_{ijkd}), \\ & \forall i \in \mathcal{V}, j \in \mathcal{V}_1, k \in \mathcal{K}, \end{aligned} \tag{6}$$

where M is a large enough constant and can be set as $\sum_{j\in\mathcal{R}_d} t^{\mathrm{U}}_{jd}$. Constraints (6) specify that the arrival time at the customer node (t_{jkd}) should exceed the sum of the arrival time at the previous customer node (t_{ikd}) and the travel time (T_{ijd}) if a customer is served.

2) Charging-related Constraints: For any $d \in \mathcal{D}$ and $i, j \in \mathcal{V}$, we use E^{w}_{ijd}, E^{s}_{ijd}, and E^{u}_{ijd} to denote the charged wireless energy, used, and unused solar energy, respectively. For any road $(i, j) \in \mathcal{E}$, we denote the rated wireless charging power of this road by $\bar{P}_{ij}$ and the wireless charging coefficient of this road in period d by η^{w}_{ijd}. We then characterize the relation between wireless and solar energy and travel time as follows.

$$E^{\mathrm{w}}_{ijd} \le T_{ijd}\bar{P}_{ij}\eta^{\mathrm{w}}_{ijd},\ \forall i \in \mathcal{V}_n, j \in \mathcal{V}_1, \tag{7a}$$

$$E^{\mathrm{s}}_{ijd} + E^{\mathrm{u}}_{ijd} = T_{ijd}\xi_{ijd},\ \forall i \in \mathcal{V}_n, j \in \mathcal{V}_1, \tag{7b}$$

which specify that the wireless energy charged is limited by the product of the rated wireless charging power and the travel time in (7a) and the available solar energy of road (i, j) equals the sum of used and unused solar energy in (7b).

For any $d \in \mathcal{D}$, $i \in \mathcal{V}$, and $k \in \mathcal{K}$, we use E_{ikd} to denote the battery level of SEV k at node i in period d, which is bounded from below and above:

$$0 \le E_{ikd} \le \bar{E}_k, \quad \forall i \in \mathcal{V}, k \in \mathcal{K}, \tag{8}$$

with $\bar{E}_k$ being the battery capacity of SEV k. The initial battery level of each SEV k (E_{v_1kd}) is specified as follows,

$$E_{v_1kd} = E_{0kd}, \quad \forall k \in \mathcal{K}. \tag{9}$$

We ensure the battery levels of each SEV at the start and end depots are equal to enable a smooth transition between any two consecutive periods:

$$E_{v_1kd} = E_{v_nkd}, \quad \forall k \in \mathcal{K}. \tag{10}$$

The battery energy dynamics of each SEV is detailed as

$$\begin{aligned} -M\left(1 - x_{ijkd}\right) \le & -E_{jkd} + E_{ikd} + E^{\mathrm{w}}_{ijd} z_{ij} + E^{\mathrm{s}}_{ijd} - e_{ijd}, \\ & \forall i \in \mathcal{V}_n, j \in \mathcal{V}_1, k \in \mathcal{K}, \end{aligned} \tag{11a}$$

$$\begin{aligned} -E_{jkd} + E_{ikd} + E^{\mathrm{w}}_{ijd} z_{ij} + E^{\mathrm{s}}_{ijd} - e_{ijd} \le & +M\left(1 - x_{ijkd}\right), \\ & \forall i \in \mathcal{V}_n, j \in \mathcal{V}_1, k \in \mathcal{K}, \end{aligned} \tag{11b}$$

where $e_{ijd} = \phi_d d_{ij}$ denotes the amount of energy consumption on road (i, j) and ϕ_d denotes the energy consumption per unit of distance. In (11), M is a large enough constant and can be set as $\sum_{k\in\mathcal{K}} \bar{E}_k$. Note that (3)–(11) hold for any $d \in \mathcal{D}$.

Remark 1. *Note that WCLs and SEVs provide two energy sources for energy replenishment, through which the charging behavior of the SEVs varies with uncertain solar charging power. To model the problem, we use a two-stage moment-based DRO model to characterize the uncertainty of solar charging power and the details of operational constraints and the objective function.*

3) Objective Function: We use ω_{T} and ω_{E} to denote the values of time and energy, respectively. For any $d \in \mathcal{D}$ and $i, j \in \mathcal{V}$, we let p_{ijd} denote the wireless charging price of road (i, j) in period d. For any $i \in \mathcal{V}$, we use c_i to denote the cost incurred when node i is visited by the SEV fleet, which may take three values: (i) vehicle usage cost $c^{\mathrm{v}} \ge 0$ at node v_1, which represents monetary loss after using SEVs (e.g., wear and tear and depreciation), (ii) zero at node v_n, and

(iii) negative value of the delivery revenue if $i \in \mathcal{R}_d$ (denoted by $D_i \leq 0$); that is,

$$c_i = \begin{cases} c^{\mathrm{v}}, 0, & \text{if } i \in \{v_1, v_n\}, \text{respectively,} \\ D_i, & \text{otherwise.} \end{cases} \tag{12}$$

The objective of the SEV operations model in period d is to minimize the operational cost consisting of (i) SEV usage cost and negative delivery revenue $\sum_{k\in\mathcal{K}}\sum_{i\in\mathcal{V}}\sum_{j\in\mathcal{V}} c_i x_{ijkd}$, (ii) cost of travel time $\sum_{k\in\mathcal{K}}\sum_{i\in\mathcal{V}}\sum_{j\in\mathcal{V}} \omega_{\mathrm{T}} T_{ijd} x_{ijkd}$, (iii) wireless charging cost $\sum_{k\in\mathcal{K}}\sum_{i\in\mathcal{V}}\sum_{j\in\mathcal{V}} p_{ijd} E^{\mathrm{w}}_{ijd} z_{ij} x_{ijkd}$, and (iv) penalty cost for unused solar power $\sum_{i\in\mathcal{V}}\sum_{j\in\mathcal{V}} \omega_{\mathrm{E}} E^{\mathrm{u}}_{ijd}$. For any $d \in \mathcal{D}$, $i, j \in \mathcal{V}$, and $k \in \mathcal{K}$, we introduce two auxiliary continuous variables f^{z}_{ijkd} and f^{x}_{ijkd} to eliminate the trilinear term in the objective function using the McCormick inequalities. Thus, the wireless charging cost $\sum_{k\in\mathcal{K}}\sum_{i\in\mathcal{V}}\sum_{j\in\mathcal{V}} p_{ijd} E^{\mathrm{w}}_{ijd} z_{ij} x_{ijkd}$ can be exactly reformulated as the following constraints,

$$(f^{\mathrm{z}}_{ijkd}, p_{ijd}E^{\mathrm{w}}_{ijd}, z_{ij}) \in M(f^{\mathrm{z}}_{ijkd}),\ \forall i \in \mathcal{V}, j \in \mathcal{V}, k \in \mathcal{K}, \tag{13a}$$
$$(f^{\mathrm{x}}_{ijkd}, f^{\mathrm{z}}_{ijkd}, x_{ijkd}) \in M(f^{\mathrm{x}}_{ijkd}),\ \forall i \in \mathcal{V}, j \in \mathcal{V}, k \in \mathcal{K}, \tag{13b}$$

where $M(f^{\mathrm{z}}_{ijkd})$ and $M(f^{\mathrm{x}}_{ijkd})$ denote the McCormick relaxation constraints (see Appendix -A) [31]. Here the McCormick relaxation is exact as both z_{ij} and x_{ijkd} are binary variables.

With the constraints and objective function above, the multi-period operation problem of SEVs is formulated as follows:

$$\begin{aligned} U_d(\boldsymbol{z}, \boldsymbol{\xi}_d) = \min_{\boldsymbol{x}_d \in \mathcal{X}_d} \sum_{k\in\mathcal{K}}\sum_{i\in\mathcal{V}}\sum_{j\in\mathcal{V}} \Big(& \big(c_i + \omega_{\mathrm{T}} T_{ijd}\big) x_{ijkd} \\ & + f^{\mathrm{x}}_{ijkd} + \omega_{\mathrm{E}} E^{\mathrm{u}}_{ijd} \Big), \end{aligned} \tag{14}$$

where $\mathcal{X}_d := \{(3)-(13)\}$ represents the feasible region of the operation problem with $\boldsymbol{x}_d = (x_{ijkd}, \forall i, j \in \mathcal{V}, k \in \mathcal{K})^\top$.

Problem 1 is a two-stage distributionally robust mixed binary linear program, which is significantly difficult to solve due to numerous binary variables (i.e., both planning and routing decisions) in both the first and second stages and the infinite-dimensional optimization problem in the second stage. In the subsequent sections, we develop outer and inner approximation models and a distributed solution method to solve Problem 1. Specifically, to handle the binary variables in the second stage, we propose an outer approximation model by leveraging LP relaxation, conic duality, and SOCP reformulation, leading to an LB for the original problem. Meanwhile, we derive three types of cuts (i.e., integer optimality cuts, subgradient cuts, and feasibility cuts) to strengthen our outer approximation model. To quantify the solution quality of the outer approximation model, with a partitioned support set, LDR, and K-adaptability reformulation, we develop an MISOCP-based inner approximation model, leading to a UB for the original problem. With the outer and inner approximation models, a distributed algorithm is devised. The underlying idea of the proposed outer and inner approximation models is illustrated in Fig. 2.

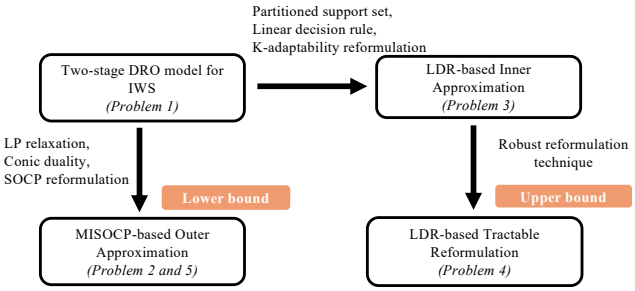

Fig. 2: Reformulation Procedures of the Outer and Inner Approximation Models.

III. Outer Approximation Model

In this section, we propose an outer approximation model that can be solved by the DCG method, by leveraging LP relaxation, conic duality, and SOCP reformulation.

For any $d \in \mathcal{D}$, we use a diagonal matrix $\boldsymbol{\Sigma}_d \in \mathbb{R}^{\vartheta\times\vartheta}$ to denote the variance matrix upper bound in (1) with every diagonal entry as σ^2_{ds} for any $s \in \{1, \ldots, \vartheta\}$ and other entries as 0. By introducing dual variables $\gamma_d \in \mathbb{R}$, $\boldsymbol{\alpha}_d \in \mathbb{R}^{\vartheta}$, $\boldsymbol{Q}_d \in \mathbb{R}^{\vartheta\times\vartheta}_+$ for the three moment constraints in (1), the second-stage maximization problem of period d, $\max_{\mathbb{P}_d\in\mathcal{P}_d} \mathbb{E}_{\mathbb{P}_d}[U_d(\boldsymbol{z}, \boldsymbol{\xi}_d)]$, can be exactly reformulated as follows [32],

$$\min_{\boldsymbol{\beta}_d}\ \gamma_d + \boldsymbol{\mu}_d{}^\top \boldsymbol{\alpha}_d + (\boldsymbol{\Sigma}_d + \boldsymbol{\mu}_d\boldsymbol{\mu}_d{}^\top) \bullet \boldsymbol{Q}_d \tag{15a}$$
$$\text{s.t. } \gamma_d + \boldsymbol{\xi}_d{}^\top \boldsymbol{\alpha}_d + \boldsymbol{\xi}_d{}^\top \boldsymbol{Q}_d \boldsymbol{\xi}_d \geq U_d(\boldsymbol{z}, \boldsymbol{\xi}_d),\ \forall \boldsymbol{\xi}_d \in S_d, \tag{15b}$$

where we let $\boldsymbol{\beta}_d := \{\gamma_d, \boldsymbol{\alpha}_d, \boldsymbol{Q}_d\}$ and $\boldsymbol{Q}_d$ is diagonal.

The computational challenge in solving (15) lies in the MILP-based value function $U_d(\boldsymbol{z}, \boldsymbol{\xi}_d)$ and the infinite number of constraints. Thus, we propose a tractable outer approximation model leveraging LP relaxation and SOCP reformulation. We use $\boldsymbol{x}^{\mathrm{b}}_d$ and $\boldsymbol{x}^{\mathrm{c}}_d$ to collect the set of binary and continuous variables in the second stage for period d, respectively. Then, the compact form of Problem (14) is presented as follows:

$$\begin{aligned} U_d(\boldsymbol{z}, \boldsymbol{\xi}_d) = \min_{\boldsymbol{x}^{\mathrm{b}}_d, \boldsymbol{x}^{\mathrm{c}}_d} \Big\{ & \boldsymbol{q}^{\mathrm{b}\top} \boldsymbol{x}^{\mathrm{b}}_d + \boldsymbol{q}^{\mathrm{c}\top} \boldsymbol{x}^{\mathrm{c}}_d : \\ & A^{\mathrm{e}} \boldsymbol{x}^{\mathrm{b}}_d = \boldsymbol{b}^{\mathrm{e}}, A^{\mathrm{i}} \boldsymbol{x}^{\mathrm{b}}_d \leq \boldsymbol{b}^{\mathrm{i}}, W^{\mathrm{ce}} \boldsymbol{x}^{\mathrm{c}}_d = \boldsymbol{h}^{\mathrm{e}}, \\ & W^{\mathrm{b}} \boldsymbol{x}^{\mathrm{b}}_d + W^{\mathrm{c}} \boldsymbol{x}^{\mathrm{c}}_d \leq \boldsymbol{h}^1 + H^2 \boldsymbol{\xi}_d + H^3 \boldsymbol{z} \Big\}. \end{aligned} \tag{16}$$

For any $d \in \mathcal{D}$, we denote the dual variables of the constraints of (16) by $\boldsymbol{\lambda}_d = \{\boldsymbol{\lambda}^{\mathrm{be}}_d, \boldsymbol{\lambda}^{\mathrm{bi}}_d \geq 0, \boldsymbol{\lambda}^{\mathrm{ce}}_d, \boldsymbol{\lambda}^{\mathrm{ci}}_d \geq 0\}$. Then, the dual problem of the LP relaxation of (16) can be represented as follows:

$$\begin{aligned} \underline{U}_d(\boldsymbol{z}, \boldsymbol{\xi}_d) = \max_{\boldsymbol{\lambda}_d} \Big\{ & - \boldsymbol{\lambda}^{\mathrm{be}\top}_d \boldsymbol{b}^{\mathrm{e}} - \boldsymbol{\lambda}^{\mathrm{bi}\top}_d \boldsymbol{b}^{\mathrm{i}} - \boldsymbol{\lambda}^{\mathrm{ce}\top}_d \boldsymbol{h}^{\mathrm{e}} \\ & - \boldsymbol{\lambda}^{\mathrm{ci}\top}_d \big(\boldsymbol{h}^1 + H^2 \boldsymbol{\xi}_d + H^3 \boldsymbol{z}\big) : \\ & A^{\mathrm{e}\top} \boldsymbol{\lambda}^{\mathrm{be}}_d + A^{\mathrm{i}\top} \boldsymbol{\lambda}^{\mathrm{bi}}_d + W^{\mathrm{b}\top} \boldsymbol{\lambda}^{\mathrm{ci}}_d + \boldsymbol{q}^{\mathrm{b}} \geq 0, \\ & W^{\mathrm{ce}\top} \boldsymbol{\lambda}^{\mathrm{ce}}_d + W^{\mathrm{c}\top} \boldsymbol{\lambda}^{\mathrm{ci}}_d + \boldsymbol{q}^{\mathrm{c}} \geq 0 \Big\}. \end{aligned} \tag{17}$$

We use F_d and $vert(F_d)$ to denote the feasible region of (17) and all the vertices of the feasible region, respectively, and φ to denote the number of such vertices. Thus, the outer

approximation formulation of semi-infinite constraints (15b) is formulated as follows:

$$\gamma_d + \boldsymbol{\xi}_d^\top \boldsymbol{\alpha}_d + \boldsymbol{\xi}_d^\top \boldsymbol{Q}_d \boldsymbol{\xi}_d \geq -\boldsymbol{\lambda}_d^{\mathrm{be}\top} \boldsymbol{b}^{\mathrm{e}} - \boldsymbol{\lambda}_d^{\mathrm{bi}\top} \boldsymbol{b}^{\mathrm{i}} - \boldsymbol{\lambda}_d^{\mathrm{ce}\top} \boldsymbol{h}^{\mathrm{e}} - \boldsymbol{\lambda}_d^{\mathrm{ci}\top} \left(\boldsymbol{h}^1 + H^2 \boldsymbol{\xi}_d + H^3 \boldsymbol{z}\right), \ \forall \boldsymbol{\lambda}_d \in \mathit{vert}(F_d), \boldsymbol{\xi}_d \in S_d. \tag{18}$$

Similar to Proposition 1 of [33], we provide an exact SDP reformulation for the semi-infinite constraints (18) in Theorem 1.

Theorem 1. *The semi-infinite constraints* (18) *can be equivalently recast as the following SDP constraint:*

$$\boldsymbol{Z}_d \succeq 0, \ \forall \boldsymbol{\lambda}_d \in \mathit{vert}(F_d), \tag{19}$$

where $\mathbf{Z}_d = \begin{bmatrix} \mathbf{Z}_d^{11} & \mathbf{Z}_d^{21\top} \\ \mathbf{Z}_d^{21} & \mathbf{Z}_d^{22} \end{bmatrix}$, $\mathbf{Z}_d^{11} = \gamma_d + \boldsymbol{\lambda}_d^{\mathrm{be}\top} \boldsymbol{b}^{\mathrm{e}} + \boldsymbol{\lambda}_d^{\mathrm{bi}\top} \boldsymbol{b}^{\mathrm{i}} + \boldsymbol{\lambda}_d^{\mathrm{ce}\top} \boldsymbol{h}^{\mathrm{e}} + \boldsymbol{\lambda}_d^{\mathrm{ci}\top} \left(\boldsymbol{h}^1 + H^3 \boldsymbol{z}\right) - \boldsymbol{\zeta}_d^\top \boldsymbol{b}_d$, $\boldsymbol{\zeta}_d \geq 0$, $\mathbf{Z}_d^{22} = \boldsymbol{Q}_d$, *and* $\mathbf{Z}_d^{21} = \frac{1}{2}(\boldsymbol{\alpha}_d + \boldsymbol{\lambda}_d^{\mathrm{ci}\top} H^2 + A_d^\top \boldsymbol{\zeta}_d)$.

Proof. We first reformulate (18) as a minimization problem:

$$\min_{\boldsymbol{\lambda}_d \in \mathit{vert}(F_d)} \min_{\boldsymbol{\xi}_d \in S_d} h(\boldsymbol{\xi}_d) \geq 0, \tag{20}$$

where $h(\boldsymbol{\xi}_d) = \gamma_d + \boldsymbol{\xi}_d{}^\top \boldsymbol{\alpha}_d + \boldsymbol{\xi}_d^\top \boldsymbol{Q}_d \boldsymbol{\xi}_d + \boldsymbol{\lambda}_d^{\mathrm{be}\top} \boldsymbol{b}^{\mathrm{e}} + \boldsymbol{\lambda}_d^{\mathrm{bi}\top} \boldsymbol{b}^{\mathrm{i}} + \boldsymbol{\lambda}_d^{\mathrm{ce}\top} \boldsymbol{h}^{\mathrm{e}} + \boldsymbol{\lambda}_d^{\mathrm{ci}\top} \left(\boldsymbol{h}^1 + H^2 \boldsymbol{\xi}_d + H^3 \boldsymbol{z}\right)$.

Given a non-negative dual vector $\boldsymbol{\zeta}_d \in \mathbb{R}^\ell$, we represent the Lagrangian dual problem of (20) as

$$\max_{\boldsymbol{\zeta}_d \geq 0} \min_{\boldsymbol{\lambda}_d \in \mathit{vert}(F_d)} \min_{\boldsymbol{\xi}_d \in \mathbb{R}^\vartheta} h(\boldsymbol{\xi}_d) + \boldsymbol{\zeta}_d^\top (A_d \boldsymbol{\xi}_d - \boldsymbol{b}_d) \geq 0,$$

which can be reformulated as follows,

$$\exists \boldsymbol{\zeta}_d \geq 0 : \gamma_d + \boldsymbol{\xi}_d^\top \boldsymbol{\alpha}_d + \boldsymbol{\xi}_d^\top \boldsymbol{Q}_d \boldsymbol{\xi}_d + \boldsymbol{\lambda}_d^{\mathrm{be}\top} \boldsymbol{b}^{\mathrm{e}} + \boldsymbol{\lambda}_d^{\mathrm{bi}\top} \boldsymbol{b}^{\mathrm{i}} + \boldsymbol{\lambda}_d^{\mathrm{ce}\top} \boldsymbol{h}^{\mathrm{e}} + \boldsymbol{\lambda}_d^{\mathrm{ci}\top} \left(\boldsymbol{h}^1 + H^2 \boldsymbol{\xi}_d + H^3 \boldsymbol{z}\right) + \boldsymbol{\zeta}_d^\top (A_d \boldsymbol{\xi}_d - \boldsymbol{b}_d) \geq 0, \quad \forall \boldsymbol{\xi}_d \in \mathbb{R}^\vartheta, \boldsymbol{\lambda}_d \in vert(F_d).$$

By the definition of a positive semi-definite (PSD) matrix, we further have the following equivalent reformulation,

$$\exists \boldsymbol{\zeta}_d \geq 0 : (1, \boldsymbol{\xi}_d^\top) \boldsymbol{Z}_d (1, \boldsymbol{\xi}_d^\top)^\top \geq 0, \ \forall \boldsymbol{\xi}_d \in \mathbb{R}^\vartheta, \boldsymbol{\lambda}_d \in vert(F_d),$$

$$\Leftrightarrow \exists \boldsymbol{\zeta}_d \geq 0 : \boldsymbol{Z}_d \succeq 0, \ \forall \boldsymbol{\lambda}_d \in vert(F_d).$$

This concludes the proof. □

Note that solving the mixed integer SDP model requires massive computational resources and time. Thus, using $\{\cdot\}_j$ and $\{\cdot\}_{jj}$ to represent the j-th entry of a vector and the j-th diagonal entry of a matrix, respectively, we further introduce the following theorem to decompose the PSD matrix (19) into smaller PSD matrices with the dimension of 2, allowing for the subsequent SOCP reformulation.

Theorem 2. *For any* $d \in \mathcal{D}$ *and* $v \in \{1, \ldots, \varphi\}$, *let* $\boldsymbol{s}_{dv} \in \mathbb{R}^\vartheta$ *denote a continuous auxiliary variable vector,* $\boldsymbol{\lambda}_{dv}$ *denote the* v*-th extreme point of vert*(F_d), *and* $\boldsymbol{Z}_{dv}$ *denote the PSD matrix corresponding to* $\boldsymbol{\lambda}_{dv}$ *in* (19). *Then,* $\boldsymbol{Z}_{dv} \succeq 0$ *is equivalent to*

- $\sum_{j=1}^{\vartheta} \{\boldsymbol{s}_{dv}\}_j = \boldsymbol{Z}_d^{11}, \{\boldsymbol{s}_{dv}\}_j \in \mathbb{R}$,
- $\begin{bmatrix} \{\boldsymbol{s}_{dv}\}_j & \{\boldsymbol{Z}_{dv}^{21}\}_j \\ \{\boldsymbol{Z}_{dv}^{21}\}_j & \{\boldsymbol{Z}_{dv}^{22}\}_{jj} \end{bmatrix} \succeq 0, \quad \forall j \in \{1, \cdots, \vartheta\}$,

for any $v \in \{1, \ldots, \varphi\}$.

Proof. See Lemma 1 of [33] for the detailed proof. □

With Theorems 1 and 2, we obtain the following MISOCP-based outer approximation model.

Problem 2 (MISOCP-based Outer Approximation)**.**

$$\min_{\substack{\boldsymbol{z} \in \mathcal{Z}, \\ \boldsymbol{\zeta}_d, \boldsymbol{\beta}_d}} \ \boldsymbol{c}^\top \boldsymbol{z} + \sum_{d \in \mathcal{D}} \left[\gamma_d + \boldsymbol{\mu}_d^\top \boldsymbol{\alpha}_d + (\boldsymbol{\Sigma}_d + \boldsymbol{\mu}_d \boldsymbol{\mu}_d^\top) \bullet \boldsymbol{Q}_d\right]$$

$$\text{s.t.} \quad \sum_{j=1}^{\vartheta} \{\boldsymbol{s}_{dv}\}_j = \boldsymbol{Z}_d^{11}, \ \forall d \in \mathcal{D}, v \in \{1, \cdots, \varphi\}, \tag{22a}$$

$$\left\| \begin{matrix} 2\{\boldsymbol{Z}_{dv}^{21}\}_j \\ \{\boldsymbol{s}_{dv}\}_j - \{\boldsymbol{Z}_{dv}^{22}\}_{jj} \end{matrix} \right\|_2 \leq \{\boldsymbol{s}_{dv}\}_j + \{\boldsymbol{Z}_{dv}^{22}\}_{jj}, \quad \forall d \in \mathcal{D}, v \in \{1, \cdots, \varphi\}, j \in \{1, \cdots, \vartheta\}. \tag{22b}$$

Note that enumerating all the vertices of $\mathit{vert}(F_d)$ is challenging. Thus, we employ a DCG method to solve Problem 2 [34]. Specifically, we solve Problem 2 with a subset of $\mathit{vert}(F_d)$ at the first iteration (leading to a relaxed problem) and then identify more vertices at the subsequent iteration by solving a feasibility subproblem. That is, in each period $d \in \mathcal{D}$, given a relaxed solution $\boldsymbol{\beta}_d$, we rearrange constraints (18) and solve the following bi-convex feasibility subproblem.

$$\begin{aligned} \min_{\boldsymbol{\lambda}_d, \boldsymbol{\xi}_d} \ & \gamma_d + \boldsymbol{\xi}_d{}^\top \boldsymbol{\alpha}_d + \boldsymbol{\xi}_d^\top \boldsymbol{Q}_d \boldsymbol{\xi}_d + \boldsymbol{\lambda}_d^{\mathrm{be}\top} \boldsymbol{b}^{\mathrm{e}} + \boldsymbol{\lambda}_d^{\mathrm{bi}\top} \boldsymbol{b}^{\mathrm{i}} \\ & + \boldsymbol{\lambda}_d^{\mathrm{ce}\top} \boldsymbol{h}^{\mathrm{e}} + \boldsymbol{\lambda}_d^{\mathrm{ci}\top} \left(\boldsymbol{h}^1 + H^2 \boldsymbol{\xi}_d + H^3 \boldsymbol{z}\right) \\ \text{s.t.} \ & \boldsymbol{\lambda}_d \in F_d, \boldsymbol{\xi}_d \in S_d, \end{aligned} \tag{23}$$

The limited number of extreme points of F_d guarantees that the DCG method can converge in a finite number of iterations (see Appendix-B for the details). Note that the DCG approach provides an LB for the original Problem 1. To quantify the solution quality of the LB, we further propose an inner approximation model that provides a UB for Problem 1 in the following section.

IV. Inner Approximation Model

In this section, we develop an inner approximation model by leveraging K-adaptability reformulation [35] and the linear decision rule [36] integrated with a partition of the support set [37], thereby obtaining a UB for Problem 1 and evaluating the quality of the LB in Section III. Note that the difficulty of solving (15) mainly comes from how to optimize the MILP-based value function $U_d(\boldsymbol{z}, \boldsymbol{\xi}_d)$. Thus, we propose a partition-based LDR approach to resolve this issue. First, for each period $d \in \mathcal{D}$, we divide the support set S_d into P_d partitions and let $\boldsymbol{P}_d := \{1, \cdots, P_d\}$. To obtain these partitions, we need to introduce ς hyperplanes. Specifically, for any $d \in \mathcal{D}$ and $p \in \boldsymbol{P}_d$, we use $B_{dp} \in \mathbb{R}^{\varsigma \times \vartheta}$ and $\boldsymbol{b}_{dp} \in \mathbb{R}^\varsigma$ to denote the coefficient matrix and the constant vector of these hyperplanes in partition p, respectively. We represent the partitioned support set S_{dp} as

$$S_{dp} = S_d \cap \{\boldsymbol{\xi}_d \mid B_{dp} \boldsymbol{\xi}_d \leq \boldsymbol{b}_{dp}\}, \ \forall p \in \boldsymbol{P}_d,$$

such that $S_d = \cup_{p \in \boldsymbol{P}_d} S_{dp}$ and $\cap_{p \in \boldsymbol{P}_d} S_{dp} = \emptyset$. Then, we adopt the K-adaptability technique [35] to separate the binary

and continuous variables in the second stage. Specifically, we denote the binary and continuous decision vector in period d of partition p by $\boldsymbol{x}^{\mathrm{b}}_{dp}$ and $\boldsymbol{x}^{\mathrm{c}}_{dp}$, respectively. We apply LDR for the continuous decision variables $\boldsymbol{x}^{\mathrm{c}}_{dp}$ as follows.

$$\boldsymbol{x}^{\mathrm{c}}_{dp} = \mathscr{A}_{dp}\boldsymbol{\xi}_d + \boldsymbol{\upsilon}_{dp},\ \forall p \in \boldsymbol{P}_d, \boldsymbol{\xi}_d \in S_{dp},$$

where $\mathscr{A}_{dp}$ and $\boldsymbol{\upsilon}_{dp}$ are the decision matrix and vector, respectively. We use $\underline{\boldsymbol{x}}^{\mathrm{c}}_d$ and $\bar{\boldsymbol{x}}^{\mathrm{c}}_d$ to denote the LB and UB of the continuous variable $\boldsymbol{x}^{\mathrm{c}}_{dp}$, respectively.

With the partition-based LDR approach, we present an inner approximation model as follows, which provides an upper bound for the original Problem 1.

Problem 3 (LDR-based Inner Approximation)**.**

$$\begin{aligned}
\min_{\boldsymbol{z}\in\mathcal{Z},\boldsymbol{x}^{\mathrm{b}}_{dp}} \ & \boldsymbol{c}^\top\boldsymbol{z} + \sum_{d\in\mathcal{D}} \max_{\mathbb{P}_d\in\mathcal{P}_d} \mathbb{E}_{\mathbb{P}_d}\left[\max_{p\in\boldsymbol{P}_d} U_{dp}(\boldsymbol{z},\boldsymbol{\xi}_d)\right] \\
\text{s.t. } & A^{\mathrm{e}}\boldsymbol{x}^{\mathrm{b}}_{dp} = \boldsymbol{b}^{\mathrm{e}}, A^{\mathrm{i}}\boldsymbol{x}^{\mathrm{b}}_{dp} \le \boldsymbol{b}^{\mathrm{i}},\ \forall d\in\mathcal{D}, p\in\boldsymbol{P}_d, && \text{(25a)}\\
& W^{\mathrm{ce}}(\mathscr{A}_{dp}\boldsymbol{\xi}_d + \boldsymbol{\upsilon}_{dp}) = \boldsymbol{h}^{\mathrm{e}}, \\
& \qquad \forall d\in\mathcal{D}, p\in\boldsymbol{P}_d, \boldsymbol{\xi}_d\in S_{dp}, && \text{(25b)}\\
& W^{\mathrm{b}}\boldsymbol{x}^{\mathrm{b}}_{dp} + W^{\mathrm{c}}(\mathscr{A}_{dp}\boldsymbol{\xi}_d + \boldsymbol{\upsilon}_{dp}) \le \boldsymbol{h}^1 + H^2\boldsymbol{\xi}_d + H^3\boldsymbol{z}, \\
& \qquad \forall d\in\mathcal{D}, p\in\boldsymbol{P}_d, \boldsymbol{\xi}_d\in S_{dp}, && \text{(25c)}\\
& \underline{\boldsymbol{x}}^{\mathrm{c}}_d \le \mathscr{A}_{dp}\boldsymbol{\xi}_d + \boldsymbol{\upsilon}_{dp} \le \bar{\boldsymbol{x}}^{\mathrm{c}}_d, \\
& \qquad \forall d\in\mathcal{D}, p\in\boldsymbol{P}_d, \boldsymbol{\xi}_d\in S_{dp}, && \text{(25d)}
\end{aligned}$$

where $U_{dp}(\boldsymbol{z},\boldsymbol{\xi}_d) = \boldsymbol{q}^{\mathrm{b}\top}\boldsymbol{x}^{\mathrm{b}}_{dp} + \boldsymbol{q}^{\mathrm{c}\top}(\mathscr{A}_{dp}\boldsymbol{\xi}_d + \boldsymbol{\upsilon}_{dp})$.

We employ robust reformulation techniques to recast $\boldsymbol{\xi}_d$-related constraints (25b)–(25d) as a set of second-order cone (SOC) and linear constraints [38], as detailed below.

1) SOCP Reformulation: The dual problem of the inner problem $\max_{\mathbb{P}_d\in\mathcal{P}_d}\mathbb{E}_{\mathbb{P}_d}[\max_{p\in\boldsymbol{P}_d} U_{dp}(\boldsymbol{z},\boldsymbol{\xi}_d)]$ can be reformulated as follows:

$$\begin{aligned}
\min_{\gamma_d,\boldsymbol{\alpha}_d,\boldsymbol{Q}_d} \ & \gamma_d + \boldsymbol{\mu}_d^\top\boldsymbol{\alpha}_d + \left(\boldsymbol{\Sigma}_d + \boldsymbol{\mu}_d\boldsymbol{\mu}_d^\top\right)\bullet\boldsymbol{Q}_d \\
\text{s.t. } & \gamma_d + \boldsymbol{\xi}_d^\top\boldsymbol{\alpha}_d + \boldsymbol{\xi}_d^\top\boldsymbol{Q}_d\boldsymbol{\xi}_d \ge U_{dp}(\boldsymbol{z},\boldsymbol{\xi}_d), \\
& \qquad \forall p\in\boldsymbol{P}_d, \boldsymbol{\xi}_d\in S_{dp}. && \text{(26)}
\end{aligned}$$

Lemma 1. *For any $d\in\mathcal{D}$ and $p\in\boldsymbol{P}_d$, let $\boldsymbol{s}_{dp}\in\mathbb{R}^\vartheta$ denote a continuous auxiliary variable vector of partition p in period d. The semi-infinite constraints* (26) *can be exactly recast as the following SOC and linear constraints,*

$$\begin{aligned}
& \left\| \begin{array}{c} 2\{\boldsymbol{Z}^{21}_{dp}\}_j \\ \{\boldsymbol{s}_{dp}\}_j - \{\boldsymbol{Z}^{22}_{dp}\}_{jj} \end{array} \right\|_2 \le \{\boldsymbol{s}_{dp}\}_j + \{\boldsymbol{Z}^{22}_{dp}\}_{jj}, \\
& \qquad \forall d\in\mathcal{D}, p\in\boldsymbol{P}_d, j\in\{1,\cdots,\vartheta\}, && \text{(27a)}\\
& \sum_{j=1}^{\vartheta}\{\boldsymbol{s}_{dp}\}_j = \boldsymbol{Z}^{11}_{dp},\ \forall d\in\mathcal{D}, p\in\boldsymbol{P}_d, && \text{(27b)}
\end{aligned}$$

where $\mathbf{Z}_{dp} = \begin{bmatrix} \mathbf{Z}^{11}_{dp} & \mathbf{Z}^{21\top}_{dp} \\ \mathbf{Z}^{21}_{dp} & \mathbf{Z}^{22}_{dp} \end{bmatrix}$, $\mathbf{Z}^{11}_{dp} = \gamma_d - \boldsymbol{q}^{\mathrm{b}\top}\boldsymbol{x}^{\mathrm{b}}_{dp} - \boldsymbol{q}^{\mathrm{c}\top}\boldsymbol{\upsilon}_{dp} - \boldsymbol{\zeta}^{\mathrm{s1}}_{dp}\boldsymbol{b}_d - \boldsymbol{\zeta}^{\mathrm{s2}}_{dp}\boldsymbol{b}_{dp})$, $\boldsymbol{\zeta}^{\mathrm{s1}}_{dp}\ge 0$, $\boldsymbol{\zeta}^{\mathrm{s2}}_{dp}\ge 0$, $\mathbf{Z}^{21}_{dp} = (1/2)(\boldsymbol{\alpha}_d + A_d^\top\boldsymbol{\zeta}^{\mathrm{s1}}_{dp} + B^\top_{dp}\boldsymbol{\zeta}^{\mathrm{s2}}_{dp} - \mathscr{A}^\top_{dp}\boldsymbol{q}^{\mathrm{c}})$, *and* $\mathbf{Z}^{22}_{dp} = \boldsymbol{Q}_d$.

Proof. See the proof in Appendix -C. □

2) Semi-infinite Equality Constraint: Constraints (25b) can be equivalently recast as the following constraints:

$$\begin{aligned}
& W^{\mathrm{ce}}\mathscr{A}_{dp} = 0,\ \forall d\in\mathcal{D}, p\in\boldsymbol{P}_d, && \text{(28a)}\\
& W^{\mathrm{ce}}\boldsymbol{\upsilon}_{dp} = \boldsymbol{h}^{\mathrm{e}},\ \forall d\in\mathcal{D}, p\in\boldsymbol{P}_d, && \text{(28b)}
\end{aligned}$$

where (28a) shows that the inner product between the coefficient and decision matrices is equal to 0 and (28b) represents the coefficients' requirement of (25b).

3) Semi-infinite Inequality Constraint: Let ϖ be the dimension of $\boldsymbol{h}^1$ and $[\cdot]_i$ denote the i-th row of a matrix or i-th entry of a vector. Constraints (25c) can be reformulated as

$$\begin{aligned}
& \left[\boldsymbol{h}^1 + H^3\boldsymbol{z} - W^{\mathrm{b}}\boldsymbol{x}^{\mathrm{b}}_{dp} - W^{\mathrm{c}}\boldsymbol{\upsilon}_{dp}\right]_i + \min_{\boldsymbol{\xi}_d\in S_{dp}}\left[H^2 - W^{\mathrm{c}}\mathscr{A}_{dp}\right]_i\boldsymbol{\xi}_d \\
& \ge 0,\ \forall d\in\mathcal{D}, p\in\boldsymbol{P}_d, i\in\{1,\ldots,\varpi\}, && \text{(29)}
\end{aligned}$$

Then, by introducing non-negative dual variables $\boldsymbol{\zeta}^{\mathrm{c1}}_{dp}\in\mathbb{R}^\ell$ and $\boldsymbol{\zeta}^{\mathrm{c2}}_{dp}\in\mathbb{R}^\varsigma$ for the constraints in S_{dp}, we dualize the inner minimization above by strong duality and reformulate (29) as

$$\begin{aligned}
& \left[\boldsymbol{h}^1 + H^3\boldsymbol{z} - W^{\mathrm{b}}\boldsymbol{x}^{\mathrm{b}}_{dp} - W^{\mathrm{c}}\boldsymbol{\upsilon}_{dp}\right]_i - \max_{\boldsymbol{\zeta}^{\mathrm{c}}_{dp}\in\Omega_{dp}}\left(\boldsymbol{b}_d^\top\boldsymbol{\zeta}^{\mathrm{c1}}_d + \boldsymbol{b}^\top_{dp}\boldsymbol{\zeta}^{\mathrm{c2}}_{dp}\right) \\
& \ge 0,\ \forall d\in\mathcal{D}, p\in\boldsymbol{P}_d, i\in\{1,\ldots,\varpi\},
\end{aligned}$$

where $\boldsymbol{\zeta}^{\mathrm{c}}_{dp} := \{\boldsymbol{\zeta}^{\mathrm{c1}}_{dp}, \boldsymbol{\zeta}^{\mathrm{c2}}_{dp}\}$ and Ω_{dp} includes $\boldsymbol{\zeta}^{\mathrm{c}}_{dp}\ge 0$ and the following constraints

$$A_d^\top\boldsymbol{\zeta}^{\mathrm{c1}}_{dp} + B^\top_{dp}\boldsymbol{\zeta}^{\mathrm{c2}}_{dp} + \left[H^2 - W^{\mathrm{c}}\mathscr{A}_{dp}\right]_i = 0,\ \forall i\in\{1,\ldots,\varpi\}.$$

As a result, constraints (29) can be recast as

$$\begin{aligned}
& \left[\boldsymbol{h}^1 + H^3\boldsymbol{z} - W^{\mathrm{b}}\boldsymbol{x}^{\mathrm{b}}_{dp} - W^{\mathrm{c}}\boldsymbol{\upsilon}_{dp}\right]_i - \boldsymbol{b}_d^\top\boldsymbol{\zeta}^{\mathrm{c1}}_d - \boldsymbol{b}^\top_{dp}\boldsymbol{\zeta}^{\mathrm{c2}}_{dp} \ge 0, \\
& \qquad \forall d\in\mathcal{D}, p\in\boldsymbol{P}_d, i\in\{1,\ldots,\varpi\}, && \text{(30a)}\\
& A_d^\top\boldsymbol{\zeta}^{\mathrm{c1}}_d + B^\top_{dp}\boldsymbol{\zeta}^{\mathrm{c2}}_{dp} + \left[H^2 - W^{\mathrm{c}}\mathscr{A}_{dp}\right]_i^\top = 0, \\
& \qquad \forall d\in\mathcal{D}, p\in\boldsymbol{P}_d, i\in\{1,\ldots,\varpi\}. && \text{(30b)}
\end{aligned}$$

4) LB and UB of Continuous Variables: For any $d\in\mathcal{D}$ and $p\in\boldsymbol{P}_d$, we let ρ_{dp} be the dimension of $\boldsymbol{\upsilon}_{dp}$ and reformulate constraints (25d) as follows (see Appendix -D for the details):

$$\begin{aligned}
& -\boldsymbol{b}_d^\top\boldsymbol{\zeta}^{\mathrm{l1}}_{dp} - \boldsymbol{b}^\top_{dp}\boldsymbol{\zeta}^{\mathrm{l2}}_{dp} + [\boldsymbol{\upsilon}_{dp}]_i - [\underline{\boldsymbol{x}}^{\mathrm{c}}_d]_i \ge 0, \\
& \qquad \forall d\in\mathcal{D}, p\in\boldsymbol{P}_d, i\in\{1,\ldots,\rho_{dp}\}, && \text{(31a)}\\
& A_d^\top\boldsymbol{\zeta}^{\mathrm{l1}}_{dp} + B^\top_{dp}\boldsymbol{\zeta}^{\mathrm{l2}}_{dp} + [\mathscr{A}_{dp}]_i^\top = 0, \\
& \qquad \forall d\in\mathcal{D}, p\in\boldsymbol{P}_d, i\in\{1,\ldots,\rho_{dp}\}, && \text{(31b)}\\
& [\bar{\boldsymbol{x}}^{\mathrm{c}}_d]_i - [\boldsymbol{\upsilon}_{dp}]_i - \boldsymbol{b}_d^\top\boldsymbol{\zeta}^{\mathrm{u1}}_{dp} - \boldsymbol{b}^\top_{dp}\boldsymbol{\zeta}^{\mathrm{u2}}_{dp} \ge 0, \\
& \qquad \forall d\in\mathcal{D}, p\in\boldsymbol{P}_d, i\in\{1,\ldots,\rho_{dp}\}, && \text{(31c)}\\
& A_d^\top\boldsymbol{\zeta}^{\mathrm{u1}}_{dp} + B^\top_{dp}\boldsymbol{\zeta}^{\mathrm{u2}}_{dp} - [\mathscr{A}_{dp}]_i^\top = 0, \\
& \qquad \forall d\in\mathcal{D}, p\in\boldsymbol{P}_d, i\in\{1,\ldots,\rho_{dp}\}. && \text{(31d)}
\end{aligned}$$

With all the techniques above, we eventually obtain the following LDR-based MISOCP reformulation for Problem 3.

Problem 4 (LDR-based Tractable Reformulation)**.**

$$\begin{aligned}
\min_{\boldsymbol{z}\in\mathcal{Z},\boldsymbol{x}^{\mathrm{b}}_{dp}} \ & \boldsymbol{c}^\top\boldsymbol{z} + \sum_{d\in\mathcal{D}}\left(\gamma_d + \boldsymbol{\mu}_d{}^\top\boldsymbol{\alpha}_d + (\boldsymbol{\Sigma}_d + \boldsymbol{\mu}_d\boldsymbol{\mu}_d^\top)\bullet\boldsymbol{Q}_d\right) \\
\text{s.t. } & \text{(25a), (27), (28), (30), (31).}
\end{aligned}$$

Here, we use DCG-LDR to refer to the approach of leveraging DCG to solve Problem 2 to obtain the LB of the original Problem 1 and employing MISOCP solvers to solve Problem 4 to obtain the UB of Problem 1. To further improve the computational performance of DCG-LDR, we provide several improvement techniques and a distributed algorithm in the following section.

V. Distributed Solution Approach

In this section, we first present three types of cuts to strengthen our outer approximation model and then propose a distributed algorithm to obtain the LB and UB of the original two-stage DRO model. Specifically, to enhance the performance of LP relaxation of the MILP-based second-stage problem (16), we derive integer optimality cuts and subgradient cuts [39] to strengthen Problem 2. Meanwhile, if the planning decision $\boldsymbol{z}$ generated by Problem 2 is infeasible to the second-stage problem of Problem 4, we further derive feasibility cuts to cut off such a planning decision.

1) Integer Optimality Cuts: We let θ be a continuous auxiliary variable for the epigraph formulation of the second-stage problem of Problem 2 and use L to denote the LB of this second-stage problem from the DCG approach. Given a planning decision $\boldsymbol{z}^*$ from the DCG approach in Section III, we use $\psi(\boldsymbol{z}^*)$ to denote the optimal value of the second-stage problem of Problem 4, which serves as the UB of the original second-stage problem of Problem 1. Let $S(z^*_{ij}) := \{(i,j) \in \mathcal{E} : z^*_{ij} = 1\}$. We define the integer optimality cut at $\boldsymbol{z}^*$ as

$$\theta \geq (\psi(\boldsymbol{z}^*) - L)\Big(\sum_{(i,j)\in S(z^*_{ij})} z_{ij} - \sum_{(i,j)\notin S(z^*_{ij})} z_{ij} - \left|S\left(z^*_{ij}\right)\right| \Big) + \psi(\boldsymbol{z}^*). \tag{33}$$

2) Subgradient Cuts: Since Problem 2 provides an outer approximation for the original Problem 1, the objective value of Problem 2 can be used to generate the subgradient cuts. Specifically, given $\boldsymbol{z}^*$, γ^*_d, $\boldsymbol{\alpha}^*_d$, and $\boldsymbol{Q}^*_d$ obtained by solving Problem 2 via our DCG method, we let $\underline{U}(\boldsymbol{z}^*) := \sum_{d\in\mathcal{D}} \left[\gamma^*_d + \boldsymbol{\mu}_d^\top \boldsymbol{\alpha}^*_d + (\boldsymbol{\Sigma}_d + \boldsymbol{\mu}_d\boldsymbol{\mu}_d^\top) \bullet \boldsymbol{Q}^*_d\right]$ denote the second-stage cost of Problem 2 at $\boldsymbol{z}^*$. We define the subgradient cut at $\boldsymbol{z}^*$ as

$$\theta \geqslant g(\boldsymbol{z}^*)(\boldsymbol{z} - \boldsymbol{z}^*) + \underline{U}(\boldsymbol{z}^*), \tag{34}$$

where $g(\boldsymbol{z}^*) = -\sum_{d\in\mathcal{D}} {\boldsymbol{\lambda}^{\mathrm{ci}}_d}^\top H^3$ denotes the subgradient of $\underline{U}(\boldsymbol{z})$ at $\boldsymbol{z}^*$.

3) Feasibility Cuts: For any $d \in \mathcal{D}$, we replace $\boldsymbol{z}^*$ involved in the second stage of Problem 4 with a local copy $\boldsymbol{y}_d \in \mathbb{R}^\vartheta$ while adding a constraint $\boldsymbol{y}_d = \boldsymbol{z}^*$ [40]. We use $\boldsymbol{\pi}_d \in \mathbb{R}^\vartheta$ to denote the vector of dual variables with respect to the constraint $\boldsymbol{y}_d = \boldsymbol{z}^*$. Thus, for any $d \in \mathcal{D}$, we obtain the following feasibility problem:

$$\max_{\boldsymbol{\pi}_d\in\mathbb{R}^\vartheta} \min_{\boldsymbol{S}_d, \boldsymbol{y}_d} \quad \mathbb{1}^\top \boldsymbol{S}_d - \boldsymbol{\pi}_d^\top(\boldsymbol{y}_d - \boldsymbol{z}^*), \tag{35}$$

where $\mathbb{1}$ denotes a column vector where every entry is 1 and $\boldsymbol{S}_d$ denotes the slack variables of all the constraints of Problem 4, i.e., (25a), (27),(28), (30), (31). Using α_z to denote the step size of the subgradient update, we leverage the subgradient method to solve the above feasibility problem [41] and update the dual variable vector as follows,

$$\boldsymbol{\pi}_d = \boldsymbol{\pi}_d + \alpha_z(\boldsymbol{y}^*_d - \boldsymbol{z}^*). \tag{36}$$

Then, given a solution of (35), denoted by $(\bar{\boldsymbol{\pi}}_d, \bar{\boldsymbol{S}}_d, \bar{\boldsymbol{y}}_d)$, we obtain the following feasibility cuts,

$$\mathbb{1}^\top \bar{\boldsymbol{S}}_d + \bar{\boldsymbol{\pi}}_d^\top(\boldsymbol{z} - \bar{\boldsymbol{y}}_d) \leq 0. \tag{37}$$

With the above three types of cuts, we obtain a strengthened outer approximation model as follows.

Problem 5 (Strengthened Outer Approximation)**.**

$$\begin{aligned} \min_{\boldsymbol{z}\in\mathcal{Z}, \boldsymbol{\zeta}_d} \quad & \boldsymbol{c}^\top \boldsymbol{z} + \theta \\ s.t. \quad & \theta \geq \sum_{d\in\mathcal{D}} \left(\gamma_d + \boldsymbol{\mu}_d{}^\top \boldsymbol{\alpha}_d + (\boldsymbol{\Sigma}_d + \boldsymbol{\mu}_d\boldsymbol{\mu}_d^\top) \bullet \boldsymbol{Q}_d\right), \\ & (22), (33), (34), (37). \end{aligned}$$

Based on the above strengthening techniques, we develop a distributed algorithm (DA) in Algorithm 1 to obtain improved LB and UB for Problem 1. Specifically, we first use the DCG method to solve our strengthened outer approximation model, i.e., Problem 5, and obtain the LB J^{o*}_L in each iteration o and then check the feasibility of the obtained planning decision $\boldsymbol{z}^{o*}$. If such a planning decision is feasible for our inner approximation model, i.e., Problem 4, then we add integer optimality cuts and subgradient cuts to Problem 5 by using the UB J^{o*}_U, which is obtained from solving Problem 4 with the given $\boldsymbol{z}^{o*}$ in a parallel over each $d \in \mathcal{D}$. Otherwise, a feasibility cut is generated to cut off this planning decision. The detailed flowchart of the proposed DA is showcased in Fig. 3.

VI. Numerical Experiments

In this section, we evaluate the performance of the centralized DCG-LDR and the distributed DA over synthetic and real transportation networks.

A. Parameter Settings

We consider the IWS problem over five periods (i.e., $\mathcal{D} = \{1, \ldots, 5\}$) and three different networks: (i) a synthetic 6-node network with $10-20$ roads, (ii) a real 8-node highway network (see Fig. 9) with 26 roads in Guangdong, China, and (iii) a real 16-node highway network (see Fig. 12) with 42 roads consisting of five provinces in Southern China. For the 6-node network, the travel distance d_{ij} is randomly taken between $10 - 100$ km for any road $(i,j) \in \mathcal{E}$. For the Guangdong network and 16-node network, we take the real distance of each road using the latitude and longitude of each city node. For any $d \in \mathcal{D}$, we let $|\mathcal{R}_d| = 2$ in the 6-node network and $|\mathcal{R}_d| = 4$ in the Guangdong and 16-node network. All the cost parameters are in USD.

We employ two SEVs for demonstration, i.e., $\mathcal{K} = \{1, 2\}$, with each having a $300\,\mathrm{kWh}$ battery and $100\,\mathrm{m}^2$ of solar panels wrapped [42]. The rated wireless charging power is set as $120\,\mathrm{kW}$ [43]. The initial battery level E_{0kd} is $240\,\mathrm{kWh}$ for any $k \in \mathcal{K}$ and $d \in \mathcal{D}$. For each SEV, the energy consumption

Algorithm 1 Distributed Algorithm

Initialization: $\boldsymbol{\lambda}_d^0$, $o = 0$, $\bar{o}$
while $o < \bar{o}$ or $(J_U^{o*} - J_L^{o*})/J_L^{o*} \leq \epsilon$ **do**
  Solve the MISOCP-based Problem 5, obtain the LB J_L^{o*} and solutions $\boldsymbol{z}^{o*}$, γ_d^{o*}, $\boldsymbol{\alpha}_d^{o*}$, and $\boldsymbol{Q}_d^{o*}$.
  for $d \in \mathcal{D}$ **do**
    Solve the feasibility problem (35) in parallel
  end for
  if $\mathbb{1}^\top \bar{\boldsymbol{S}}_d \leq 0$ for all $d \in \mathcal{D}$ **then**
    Obtain the UB J_U^{o*} and add the integer optimality cuts (33) and subgradient cuts (34) to Problem 5
  else
    Add the feasibility cuts (37) to Problem 5
  end if
  for $d \in \mathcal{D}$ **do**
    Given the obtained solution $\boldsymbol{z}^{o*}$, γ_d^{o*}, $\boldsymbol{\alpha}_d^{o*}$, and $\boldsymbol{Q}_d^{o*}$, solve the biconvex problem (23) in parallel, resulting in the optimal value r_d^{o*} and optimal solution $\boldsymbol{\lambda}_d^{o*}$.
  end for
  if $r_d^{o*} \geq 0$ for all $d \in \mathcal{D}$ **then**
    return J_L^{o*} is the optimal value for the outer approximation model (Problem 5)
  else
    Enlarge the vertex sets of the dual feasible region F_d, $\boldsymbol{\lambda}_d^{o+1} = \boldsymbol{\lambda}_d^o \cup \{\boldsymbol{\lambda}_d^{o*} : r_d^{o*} < 0\}$
  end if
  $o = o + 1$
end while

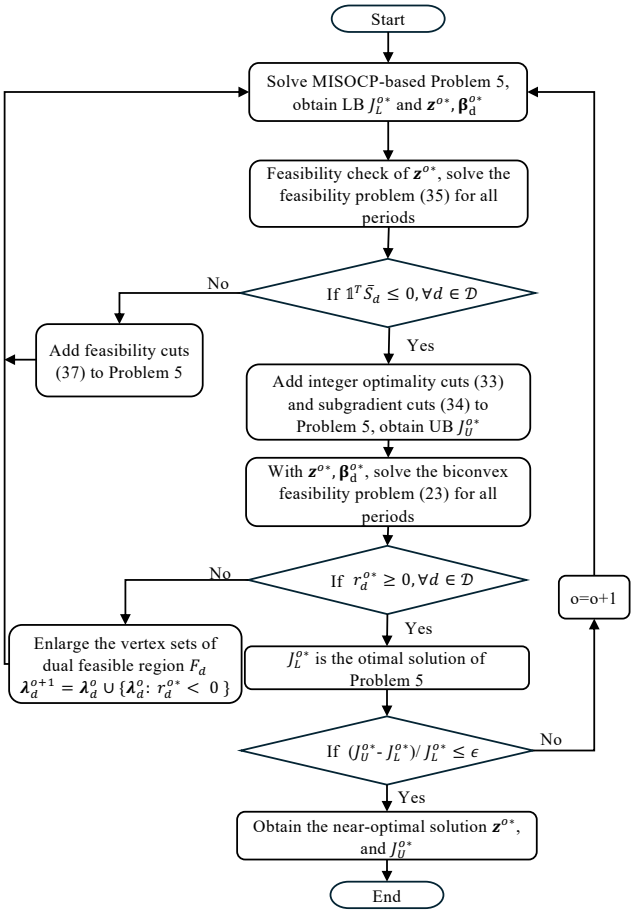

Fig. 3: Flowchart of the Proposed DA.

rate ϕ_d is set as 0.2 kW h/km [44] for any $d \in \mathcal{D}$ and the travel speed is uniformly sampled between $50 - 70$ km/h, by which we obtain the travel time T_{ijd} of each road $(i, j) \in \mathcal{E}$ in period $d \in \mathcal{D}$. The usage cost c^{v} of each SEV is set as 199. We sample the delivery revenue $-D_i$ for each $i \in \mathcal{R}_d$ and $d \in \mathcal{D}$ from a truncated normal distribution with a mean of 9.05 and a standard deviation of 5. The values of time ω_{T} and energy ω_{E} are set as 60 and 1, respectively.

The deployment cost per km for a WCL is 1.55 million [45]. The charging price of a WCL is uniformly generated between 1 and 10 for each period. The wireless charging coefficient of WCLs η_{ijd}^{w} for each period is 0.99. We obtain solar power data from the Photovoltaic Geographical Information System [46]. We let $\underline{\boldsymbol{\xi}}_d$ and $\bar{\boldsymbol{\xi}}_d$ denote the lower and upper bounds of solar power samples for each $d \in \mathcal{D}$, respectively, which are used to obtain the values of A_d and $\boldsymbol{b}_d$ in S_d. For our LDR-based inner approximation, we partition the support set S_d into two parts for each $d \in \mathcal{D}$ by using a hyperplane with $B_{dp} := \mathbb{1}_\vartheta^\top$ and $\boldsymbol{b}_{dp} := (1/2)\mathbb{1}_\vartheta^\top \bar{\boldsymbol{\xi}}_d$. The subscript of $\mathbb{1}$ denotes the dimensions of the column vector whose entries all are 1. To solve the feasibility problem (35), we update the subgradient $\boldsymbol{\pi}_d$ in (36) by using the nonsummable diminishing step size rule [41], i.e., $\alpha_z(k) = 0.05/\sqrt{k}$, where k denotes the number of iterations of the subgradient method. The details of parameter settings can be found in Table II.

All numerical experiments are executed on a Lenovo workstation with Intel(R) Xeon(R) W-2195 CPU 2.30 GHz and 128 GB of RAM. All optimization models are solved by Gurobi 11.0.1 with Python 3.9.6. The computational time limit for both DCG-LDR and DA is set as 36000 seconds for each run. Each numerical test is repeated 10 times over the randomly generated parameters above (e.g., travel speeds, delivery revenues, and wireless charging prices).

TABLE II: Parameter Settings

Parameter	Value	Parameter	Value
c_{ij}	1.55 million/km	D_i	9.05 \$
$\bar{P}_{ij}$	120 kW	ω_{T}	60
ω_{E}	1	ϕ_d	0.2 kWh/km
$\bar{E}$	300 kW h	p_{ijd}	1-10 \$
E_{0kd}	240 kW h	Speed	50-70 km/h
c^{v}	199 \$	Distance	10-100 km

B. Computational Performance

We examine the computational performance of our proposed methods over the synthetic 6-node network by varying the penetration rate of WCLs ($\underline{C}$) from 0.4 to 0.6. We use box plots to illustrate the distribution of numerical results, including the optimality gap and computational times.

First, the DCG algorithm solves the MISOCP-based outer approximation model very fast with a computational time less than 0.06 s over all instances (see Fig. 4) and has a fast convergence within around two iterations. In addition, Table III

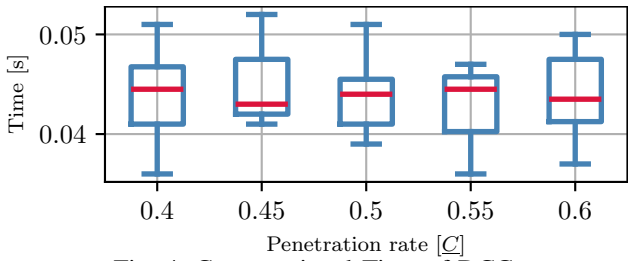

Fig. 4: Computational Time of DCG.

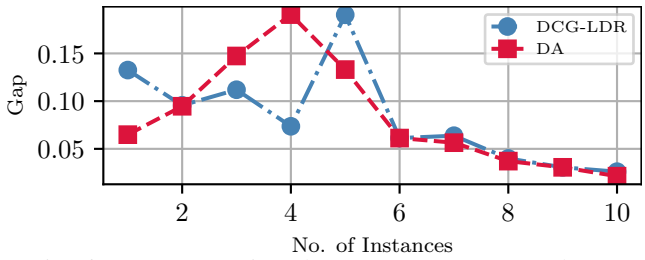

Fig. 6: Gap Comparison between DCG-LDR and DA.

shows that the LDR-based inner approximation model is more difficult to solve, while all instances are solved to optimality within the time limit.

TABLE III: Numerical Results of LDR-based Reformulation

Penetration rate ($\underline{C}$)	0.40	0.45	0.50	0.55	0.60
Time (s)	2926.01	5733.85	3430.98	4504.13	6540.64
Gap	0	0	0	0	0

Second, we obtain the optimality gap of DCG-LDR by using the LB from the outer approximation solved by the DCG method and the UB from the LDR-based inner approximation. Fig. 5 shows that the median optimality gap over ten instances (the values of the red lines) is smaller than 0.1 under different penetration rates ($\underline{C}$), showcasing good solution quality of our proposed solution methods.

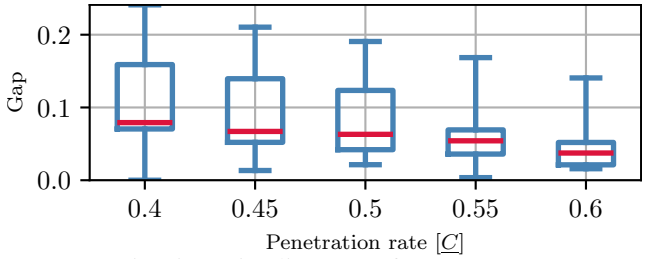

Fig. 5: Optimality Gap of DCG-LDR.

Third, we compare the above centralized DCG-LDR method with our proposed DA method (see Section V), which provides a distributed implementation and fits practical scenarios well. We fix the penetration rate ($\underline{C}$) at 0.5 and compare the optimality gap between DA and DCG-LDR for each of the ten instances. Fig. 6 shows that DA performs better than the DCG-LDR in reducing the optimality gap, with 7 out of 10 instances obtaining a lower optimality gap thanks to our proposed strengthening techniques in Section V. In addition, when varying the penetration rate ($\underline{C}$) from 0.4 to 0.6, we have the average computational times of DA are $\{2355.32, 2676.57, 2066.09, 1846.74, 1717.52\}$ seconds, respectively, significantly faster than the LDR-based reformulation in Table III.

Fourth, to assess the scalability of the proposed method, we evaluate the proposed DA method on an 8-node transportation network. The evaluation is conducted by increasing the number of roads from 22 to 28, with the penetration rate of WCL fixed as 0.4. As shown in Fig. 7, the median computational time rises from 100 s to 1000 s as the number of roads increases from 22 to 28, while the number of iterations remains consistently low, ranging between 2 and 3.

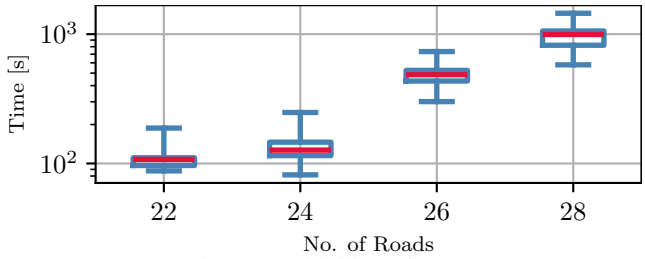

Fig. 7: Scalability of DA.

C. Case Study

We further examine the performance of our proposed model under the DA method over the highway network of Guangdong. The wireless charging coefficients of WCLs are uniformly generated between 80% and 100%. First, through varying different penetration rates of WCLs ($\underline{C}$), we observe from Fig. 8 that the DA method continues to perform well on the real transportation network, with the median optimality gap below 0.075 across all instances. Then, we mainly consider different wireless charging power rates of WCLs and different battery capacities of SEVs to obtain the WCL planning decisions. Fig. 9 and 10 show the results. The dashed and solid green lines denote the roads without and with WCLs, respectively. The two (bigger) blue nodes (*Zhanjiang* and *Shantou*) and red nodes denote the depots and customers, respectively.

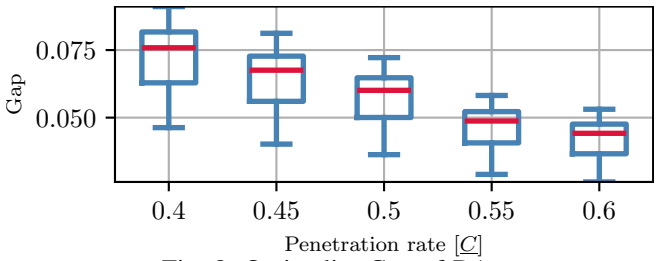

Fig. 8: Optimality Gap of DA.

1) Wireless Charging Power and Solar Power: To assess the impact of wireless charging power rate on the WCL planning decisions, we evaluate the proposed model with two different types of WCLs: 20 kW WCLs and 120 kW WCLs. Fig. 9 shows that the number of WCLs can be reduced with the larger wireless charging power (120 kW). Compared to

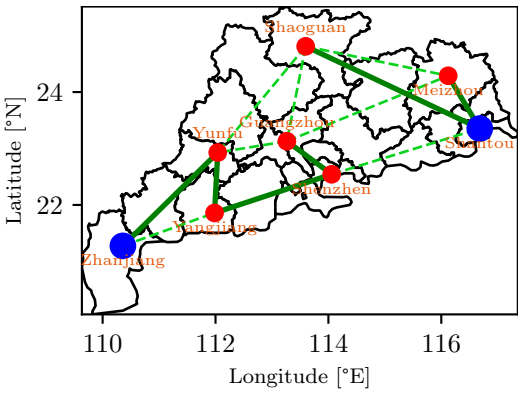

(a) 20 kW wireless charging power

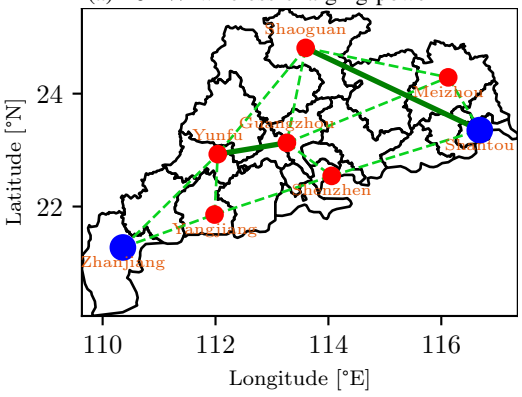

(b) 120 kW wireless charging power

Fig. 9: WCL Planning Decisions with Different Wireless Charging Power Rates.

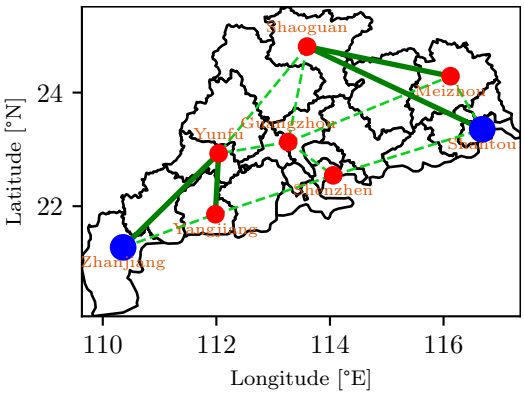

(a) 100 kW h battery capacity

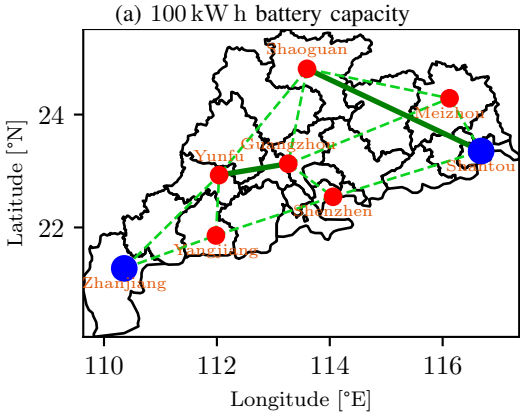

(b) 300 kW h battery capacity

Fig. 10: WCL Planning Decisions with Different Battery Capacities.

the 20 kW WCLs, the 120 kW WCLs allow more energy to be replenished for SEVs, which in turn reduces the number of planned WCLs. We also examine the impact of solar power on the WCL planning decisions and observe that more WCLs are required when the peak solar power decreases along the *Shaoguan-Meizhou* road and remains unchanged along other roads. This indicates that additional WCLs are needed in areas with lower solar power availability.

2) Battery Capacity: To assess the impact of different battery capacities on the WCL planning decisions, we evaluate the proposed model using two different types of SEVs: 100 kW h SEVs and 300 kW h SEVs. Fig. 10 shows that SEVs with a larger battery capacity of 300 kW h require fewer WCLs for the energy replenishment. Specifically, SEVs with large batteries can store significant solar energy, thereby reducing their reliance on the wireless charging power from WCLs.

We further perform a cost comparison considering different wireless charging power rates and battery capacities together and report the results in Table IV. In the table, "1st Cost" and "2nd Cost" represent the costs incurred in the first and second stages, respectively. Cases 1 and 2 in the table demonstrate that more WCLs are required when the wireless charging power decreases from 120 kW to 20 kW (see the detailed planning decisions in Fig. 9). We also observe that an increased battery capacity contributes to the reduction of the first-stage cost by comparing the results of Cases 1 and 3 (see the detailed planning decisions in Fig. 10).

TABLE IV: Cost Comparison with Different Wireless Charging Power Rates and Battery Capacities

Case	Wireless Power (kW)	Battery Capacity (kW h)	1st Cost (million)	2nd Cost (million)	Total Cost (million)
1	120	300	64.72	316.88	381.60
2	20	300	278.76	320.02	598.78
3	120	100	178.87	319.96	498.83

3) Energy Consumption Rate: To assess the robustness of the proposed model concerning different energy consumption rates, we evaluate our model by varying the energy consumption rate of SEVs from 0.1 kWh/km to 0.3 kWh/km. As a larger energy consumption rate results in an increasing demand for energy replenishment, more WCLs are built when the consumption rate is larger than 0.25 kWh/km and compared to a smaller energy consumption rate, such as 0.1 kWh/km and 0.15 kWh/km. Meanwhile, the objective value of the proposed model slightly increases from 380.90 to 408.89 million when the energy consumption rate increases (see Table V). Nevertheless, the minor increment of the objective value showcases that our proposed model can provide robust solutions with varying energy consumption rates.

4) Conservativeness of the Proposed Method: To examine the conservativeness of the proposed DRO model, we compare it with the well-known sample average approximation (SAA) model. Leveraging the SAA model, we can formulate Problem 1 as a mixed binary linear program, which can be

TABLE V: Cost Comparison with Different Energy Consumption Rates

Case	Energy Consumption Rate (kW h/km)	1st cost (million)	2nd cost (million)	Total Cost (million)
1	0.10	64.72	316.18	380.90
2	0.15	64.72	316.53	381.25
3	0.20	64.72	316.88	381.60
4	0.25	91.09	317.26	408.35
5	0.30	91.09	317.80	408.89

directly solved using optimization solvers. To perform the comparison, we generate 10 instances. First, for each instance, we generate 200 data samples and divide them equally into two datasets: a training dataset and a testing dataset, following the requirements of the moment-based ambiguity set (1). The planning decisions of the SAA and DRO models ($\boldsymbol{z}^{\mathrm{S}}$, $\boldsymbol{z}^{\mathrm{D}}$) are generated using the training dataset, leading to in-sample tests. Then, we evaluate the performance of these planning decisions on the testing dataset, leading to out-of-sample tests. Here, we define the objective values of the SAA and DRO models as J^{S} and J^{D}, respectively. We further define the conservativeness metric as $\frac{J^{\mathrm{D}}-J^{\mathrm{S}}}{J^{\mathrm{S}}} \times 100\%$. In Fig. 11, we illustrate the in-sample results of these two models on the training dataset, showing that the conservativeness value of DRO is less than 2%. Nevertheless, the conservativeness value on the testing dataset is negative, indicating that J^{S} is larger than J^{D}, with the absolute value ranging from 0.94% to 1.17%. The results show that the DRO model achieves better out-of-sample performance than the SAA model. The in-sample performance of SAA is better than DRO because the latter provides a relatively conservative solution on the training dataset and thus generates a higher total cost. However, such a conservative solution helps the DRO model hedge against potential worst-case scenarios on the testing dataset, leading to a lower total cost than the SAA model, which cannot protect one from worst-case scenarios. Thus, the DRO model achieves a better out-of-sample performance than the SAA model.

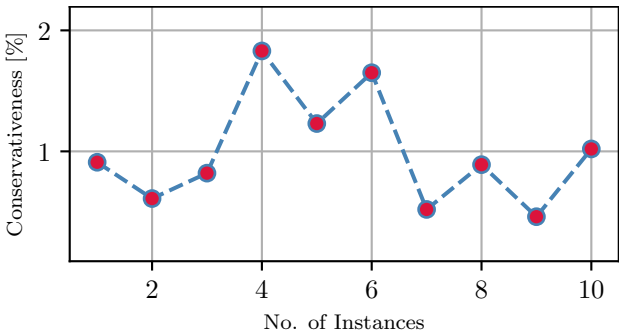

Fig. 11: In-sample Performance of DRO and SAA.

5) Comparison with Sample Average Approximation (SAA) Method on a 16-node Network: We further evaluate the proposed model on a 16-node transportation network with 42 roads, consisting of five provinces in China (Guangdong, Guangxi, Guizhou, Hunan, Jiangxi), to showcase the scalability of the proposed method in comparison with the SAA model. In Fig. 12, we show the detailed topology of the 16-node network, in which two (bigger) blue nodes (*Shantou* and *Guilin*) represent the start and end depots, respectively.

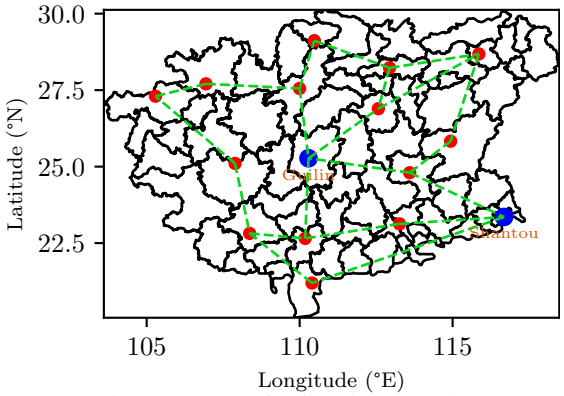

Fig. 12: Map of 16-node network.

Here, we generate 10 instances, and for each instance, we generate 10 data samples and divide them equally into two datasets: a training dataset and a testing dataset, following the requirements of the moment-based ambiguity set (1). The computational times of the SAA and DRO models are illustrated in Fig. 13. The conservativeness value of the DRO model ranges between 0.68% and 2.06% on the training dataset. The corresponding conservativeness value on the testing dataset is negative, indicating that J^{S} is larger than J^{D}, with an average absolute value of 0.55 % across the 10 instances. The results show that the DRO model achieves better out-of-sample performance than SAA on the 16-node network. More importantly, the computational time of solving the DRO model is consistently shorter than that of solving the SAA model for each instance. Specifically, the computational time of SAA reaches the time limit with an average terminating gap of 0.46%. Given that the computational time of solving the SAA model increases significantly as the number of data samples increases, our proposed DRO model demonstrates superior computational efficiency, particularly when a large number of data samples are involved.

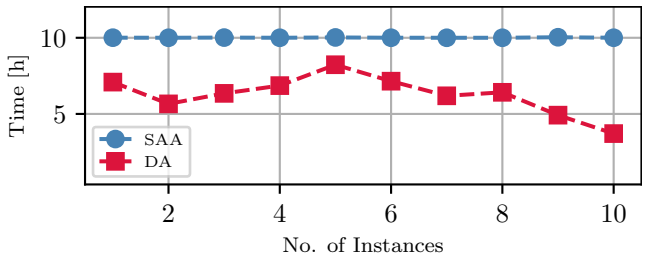

Fig. 13: Computational Time of DA and SAA.

VII. Conclusion

Motivated by (i) the slow charging power and limited battery capacity of EVs, (ii) the range anxiety of customers, and (iii) the growing development of WCLs and SEVs, we investigate the optimal planning of WCLs while considering the optimal operations of SEVs under uncertain solar power harvesting. Given available solar power data, we propose a data-driven two-stage DRO model for this integrated WCL

planning and SEV operations problem. Such a model involves numerous binary variables in both stages (location and routing variables) and an infinite-dimensional optimization problem in the second stage, leading to a significant computational challenge. To address this challenge, we design an MISOCP-based outer approximation model by leveraging the techniques of LP relaxation and SDP reformulation and an inner approximation model by employing a partitioned support set and LDR, leading to an LB and a UB for the original problem, respectively. To improve the approximation solution quality, we strengthen our outer approximation by using integer optimality, subgradient, and feasibility cuts and further design a distributed approach for parallel implementation.

We conduct extensive numerical experiments with synthetic and real transportation networks to demonstrate the effectiveness and scalability of our proposed model and solution approaches. Our findings demonstrate that the proposed DRO model achieves a 1.17% lower total cost in out-of-sample tests than the SAA model, underscoring its superior effectiveness in practical application. With higher wireless charging power rates and increased battery capacities, we can build fewer WCLs.

In the future, this paper can be extended in various directions. First, since solar power varies across different locations over a road, it would be interesting yet challenging to accurately characterize the uncertain solar charging power at all the specific locations along a road. Second, given that the performance of our two-stage DRO model depends on how we construct the ambiguity set, it would be promising to leverage machine learning methods to construct a reliable ambiguity set from historical data. Third, it would also be intriguing to consider more intricate elements (such as a fleet of SEVs with diverse capacities) in our proposed model and further improve the corresponding approximation algorithms. We leave these for future research.

APPENDIX

A. McCormick Relaxation Method

Given a bilinear term xy with $x^{\mathrm{L}} \le x \le x^{\mathrm{U}}$ and $y^{\mathrm{L}} \le y \le y^{\mathrm{U}}$, we introduce a continuous auxiliary variable z and let $z = xy$. Then, the McCormick envelope reformulation is shown as follows:

$$M(z,x,y) = \begin{cases} z \ge x^{\mathrm{L}}y + xy^{\mathrm{L}} - x^{\mathrm{L}}y^{\mathrm{L}}, \\ z \ge x^{\mathrm{U}}y + xy^{\mathrm{U}} - x^{\mathrm{U}}y^{\mathrm{U}}, \\ z \le x^{\mathrm{U}}y + xy^{\mathrm{L}} - x^{\mathrm{U}}y^{\mathrm{L}}, \\ z \le xy^{\mathrm{U}} + x^{\mathrm{L}}y - x^{\mathrm{L}}y^{\mathrm{U}}. \end{cases}$$

B. Detailed DCG Algorithm

Algorithm 2 DCG Algorithm

1: Initialization: $\boldsymbol{\lambda}_d^0$, $o = 0$, $\bar{o}$,
2: Find initial sets of vertices of the dual feasible region $\boldsymbol{\lambda}_d^o$ for each period d
3: **while** $o < \bar{o}$ **do**
4: Solve the MISOCP-based **Problem 2,** obtain the LB J_L^{o*}, and solutions $\boldsymbol{z}^{o*}, \gamma_d^{o*}, \boldsymbol{\alpha}_d^{o*}, \boldsymbol{Q}_d^{o*}$.
5: **for** $d \in \mathcal{D}$ **do**
6: Given the solution of $\boldsymbol{z}^{o*}, \gamma_d^{o*}, \boldsymbol{\alpha}_d^{o*}, \boldsymbol{Q}_d^{o*}$, solve the biconvex problem (23), resulting in the optimal values r_d^{o*} and optimal solutions $\boldsymbol{\lambda}_d^{o*}$.
7: **end for**
8: **if** $r_d^{o*} \ge 0, \forall d \in \mathcal{D}$ **then**
9: **return** J_L^{o*} is the optimal solution for the outer approximation model (Problem 2)
10: **else**
11: Enlarge the vertex sets of the dual feasible region F_d, $\boldsymbol{\lambda}_d^{o+1} = \boldsymbol{\lambda}_d^o \cup \{\boldsymbol{\lambda}_d^{o*} : r_d^{o*} < 0\}$
12: **end if**
13: $o = o + 1$
14: **end while**

C. Proof of Lemma1

Proof. The semi-infinite constraint (26) can be recast as the following constraint,

$$\gamma_d \ge \max_{\boldsymbol{\xi}_d \in S_{dp}} \left\{ U_{dp}(\boldsymbol{z}, \boldsymbol{\xi}_d) - {\boldsymbol{\xi}_d}^{\top} \boldsymbol{\alpha}_d - \boldsymbol{\xi}_d^{\top} \boldsymbol{Q}_d \boldsymbol{\xi}_d \right\}, \quad \forall p \in \boldsymbol{P}_d, \tag{A1}$$

Substituting $U_{dp}(\boldsymbol{z}, \boldsymbol{\xi}_d)$ into (A1) becomes

$$\begin{aligned} \gamma_d \ge \max_{\boldsymbol{\xi}_d \in S_{dp}} \Big\{ & {\boldsymbol{q}^{\mathrm{b}}}^{\top} \boldsymbol{x}_{dp}^{\mathrm{b}} + {\boldsymbol{q}^{\mathrm{c}}}^{\top} (\mathscr{A}_{dp} \boldsymbol{\xi}_d + \boldsymbol{\upsilon}_{dp}) - {\boldsymbol{\xi}_d}^{\top} \boldsymbol{\alpha}_d \\ & - \boldsymbol{\xi}_d^{\top} \boldsymbol{Q}_d \boldsymbol{\xi}_d \Big\}, \quad \forall p \in \boldsymbol{P}_d, \end{aligned} \tag{A2}$$

Constraints (A2) can be further recast as follows,

$$\begin{aligned} \min_{\boldsymbol{\xi}_d \in \mathbb{R}^{\vartheta}} \Big\{ & \gamma_d - {\boldsymbol{q}^{\mathrm{b}}}^{\top} \boldsymbol{x}_{dp}^{\mathrm{b}} - {\boldsymbol{q}^{\mathrm{c}}}^{\top} (\mathscr{A}_{dp} \boldsymbol{\xi}_d + \boldsymbol{\upsilon}_{dp}) \\ & + {\boldsymbol{\xi}_d}^{\top} \boldsymbol{\alpha}_d + \boldsymbol{\xi}_d^{\top} \boldsymbol{Q}_d \boldsymbol{\xi}_d \Big\} \ge 0, \quad \forall p \in \boldsymbol{P}_d. \end{aligned} \tag{A3}$$

By introducing nonnegative dual variable vectors $\boldsymbol{\zeta}_{dp}^{\mathrm{s1}} \in \mathbb{R}^{\ell}$ and $\boldsymbol{\zeta}_{dp}^{\mathrm{s2}} \in \mathbb{R}^{\varsigma}$ for the constraints in S_{dp}, the Lagrangian dual problem of (A3) is formulated as follows,

$$\max_{\boldsymbol{\zeta}_{dp}^{\mathrm{s1}} \ge 0, \boldsymbol{\zeta}_{dp}^{\mathrm{s2}} \ge 0} \min_{\boldsymbol{\xi}_d \in \mathbb{R}^{\vartheta}} H_p(\boldsymbol{\xi}_d) \ge 0, \quad \forall p \in \boldsymbol{P}_d, \tag{A4}$$

where

$$\begin{aligned} H_p(\boldsymbol{\xi}_d) = & \gamma_d - {\boldsymbol{q}^{\mathrm{b}}}^{\top} \boldsymbol{x}_{dp}^{\mathrm{b}} - {\boldsymbol{q}^{\mathrm{c}}}^{\top} (\mathscr{A}_{dp} \boldsymbol{\xi}_d + \boldsymbol{\upsilon}_{dp}) + {\boldsymbol{\xi}_d}^{\top} \boldsymbol{\alpha}_d \\ & + \boldsymbol{\xi}_d^{\top} \boldsymbol{Q}_d \boldsymbol{\xi}_d + \boldsymbol{\zeta}_{dp}^{\mathrm{s1}} (A_d \boldsymbol{\xi}_d - \boldsymbol{b}_d) + \boldsymbol{\zeta}_{dp}^{\mathrm{s2}} (B_{dp} \boldsymbol{\xi}_d - \boldsymbol{b}_{dp}). \end{aligned}$$

The max-min problem (A4) can be further recast as

$$\exists \boldsymbol{\zeta}_{dp}^{\mathrm{s1}} \ge 0, \boldsymbol{\zeta}_{dp}^{\mathrm{s2}} \ge 0 : H_p(\boldsymbol{\xi}_d) \ge 0, \ \forall \boldsymbol{\xi}_d \in \mathbb{R}^{\vartheta}, p \in \boldsymbol{P}_d. \tag{A5}$$

Then, we have the following PSD constraints,

$$\begin{aligned} & \exists \boldsymbol{\zeta}_{dp}^{\mathrm{s1}} \ge 0, \boldsymbol{\zeta}_{dp}^{\mathrm{s2}} \ge 0, \quad (1, \boldsymbol{\xi}_d^{\top}) \boldsymbol{Z}_{dp} (1, \boldsymbol{\xi}_d^{\top})^{\top} \ge 0, \\ & \qquad \forall \boldsymbol{\xi}_d \in \mathbb{R}^{\vartheta}, p \in \boldsymbol{P}_d, \\ \Leftrightarrow & \exists \boldsymbol{\zeta}_{dp}^{\mathrm{s1}} \ge 0, \boldsymbol{\zeta}_{dp}^{\mathrm{s2}} \ge 0, \quad \boldsymbol{Z}_{dp} \succeq 0, \quad \forall p \in \boldsymbol{P}_d, \end{aligned}$$

where $\mathbf{Z}_{dp} = \begin{bmatrix} \mathbf{Z}_{dp}^{11} & \mathbf{Z}_{dp}^{21\top} \\ \mathbf{Z}_{dp}^{21} & \mathbf{Z}_{dp}^{22} \end{bmatrix}$, $\mathbf{Z}_{dp}^{11} = \gamma_d - {\boldsymbol{q}^{\mathrm{b}}}^{\top} \boldsymbol{x}_{dp}^{\mathrm{b}} - {\boldsymbol{q}^{\mathrm{c}}}^{\top} \boldsymbol{\upsilon}_{dp} - \boldsymbol{\zeta}_{dp}^{\mathrm{s1}} \boldsymbol{b}_d - \boldsymbol{\zeta}_{dp}^{\mathrm{s2}} \boldsymbol{b}_{dp}), \boldsymbol{\zeta}_{dp}^{\mathrm{s1}} \ge 0, \boldsymbol{\zeta}_{dp}^{\mathrm{s2}} \ge 0$, $\mathbf{Z}_{dp}^{21} = \frac{1}{2} \Big(\boldsymbol{\alpha}_d + A_d^{\top} \boldsymbol{\zeta}_{dp}^{\mathrm{s1}} + B_{dp}^{\top} \boldsymbol{\zeta}_{dp}^{\mathrm{s2}} - \mathscr{A}_{dp}^{\top} \boldsymbol{q}^{\mathrm{c}} \Big)$, and $\mathbf{Z}_{dp}^{22} = \boldsymbol{Q}_d$. □

D. Robust Reformulation of LB and UB of Continuous Variables

By leveraging robust optimization techniques, constraints (25d) can be reformulated as linear constraints.

1) LB-constraint Reformulation: The LB of (25d) can be reformulated as follows,

$$\begin{aligned}\min_{\boldsymbol{\xi}_d\in S_{dp}} \left([\mathscr{A}_{dp}]_i\,\boldsymbol{\xi}_d\right) + [\boldsymbol{\upsilon}_{dp}]_i - [\underline{\boldsymbol{x}}^{\mathrm{c}}_d]_i \geq 0,\\ \forall d\in\mathcal{D}, p\in\boldsymbol{P}_d, i\in\{1,\ldots,\rho_{dp}\}.\end{aligned} \tag{A7}$$

By introducing nonnegative dual variable vectors $\boldsymbol{\zeta}^{\mathrm{l1}}_{dp}\in\mathbb{R}^{\ell}$ and $\boldsymbol{\zeta}^{\mathrm{l2}}_{dp}\in\mathbb{R}^{\varsigma}$ for the constraints in S_{dp}, we dualize the inner minimization problem above by strong duality and reformulate (A7) as

$$\begin{aligned}\max_{\boldsymbol{\zeta}^{\mathrm{l}}_{dp}\in\Omega^{\mathrm{l}}_{dp}} \left(-\boldsymbol{b}_d^{\top}\boldsymbol{\zeta}^{\mathrm{l1}}_{dp} - \boldsymbol{b}_{dp}^{\top}\boldsymbol{\zeta}^{\mathrm{l2}}_{dp}\right) + [\boldsymbol{\upsilon}_{dp}]_i - [\underline{\boldsymbol{x}}^{\mathrm{c}}_d]_i \geq 0,\\ \forall d\in\mathcal{D}, p\in\boldsymbol{P}_d, i\in\{1,\ldots,\rho_{dp}\}.\end{aligned} \tag{A8}$$

where $\boldsymbol{\zeta}^{\mathrm{l}}_{dp} := \{\boldsymbol{\zeta}^{\mathrm{l1}}_{dp}, \boldsymbol{\zeta}^{\mathrm{l2}}_{dp}\}$ and Ω^{l}_{dp} includes $\boldsymbol{\zeta}^{\mathrm{l}}_{dp}\geq 0$ and the following constraints

$$\begin{aligned}A_d^{\top}\boldsymbol{\zeta}^{\mathrm{l1}}_{dp} + B_{dp}^{\top}\boldsymbol{\zeta}^{\mathrm{l2}}_{dp} + [\mathscr{A}_{dp}]_i^{\top} = 0,\\ \forall d\in\mathcal{D}, p\in\boldsymbol{P}_d, i\in\{1,\ldots,\rho_{dp}\}.\end{aligned}$$

Constraints (A8) are further recast as

$$\begin{aligned}&-\boldsymbol{b}_d^{\top}\boldsymbol{\zeta}^{\mathrm{l1}}_{dp} - \boldsymbol{b}_{dp}^{\top}\boldsymbol{\zeta}^{\mathrm{l2}}_{dp} + [\boldsymbol{\upsilon}_{dp}]_i - [\underline{\boldsymbol{x}}^{\mathrm{c}}_d]_i \geq 0,\\ &\qquad\forall d\in\mathcal{D}, p\in\boldsymbol{P}_d, i\in\{1,\ldots,\rho_{dp}\},\end{aligned} \tag{A9a}$$

$$\begin{aligned}&A_d^{\top}\boldsymbol{\zeta}^{\mathrm{l1}}_{dp} + B_{dp}^{\top}\boldsymbol{\zeta}^{\mathrm{l2}}_{dp} + [\mathscr{A}_{dp}]_i^{\top} = 0,\\ &\qquad\forall d\in\mathcal{D}, p\in\boldsymbol{P}_d, i\in\{1,\ldots,\rho_{dp}\}.\end{aligned} \tag{A9b}$$

2) UB-constraint Reformulation: The UB of (25d) can be reformulated as follows,

$$\begin{aligned}[\bar{\boldsymbol{x}}^{\mathrm{c}}_d]_i - [\boldsymbol{\upsilon}_{dp}]_i + \min_{\boldsymbol{\xi}_d\in S_{dp}} \left(-[\mathscr{A}_{dp}]_i\,\boldsymbol{\xi}_d\right) \geq 0,\\ \forall d\in\mathcal{D}, p\in\boldsymbol{P}_d, i\in\{1,\ldots,\rho_{dp}\}.\end{aligned} \tag{A10}$$

By introducing dual variable vectors $\boldsymbol{\zeta}^{\mathrm{u1}}_{dp}\in\mathbb{R}^{\ell}$ and $\boldsymbol{\zeta}^{\mathrm{u2}}_{dp}\in\mathbb{R}^{\varsigma}$ for the constraints in S_{dp}, we dualize the inner minimization problem above by strong duality and reformulate (A10) as

$$\begin{aligned}[\bar{\boldsymbol{x}}^{\mathrm{c}}_d]_i - [\boldsymbol{\upsilon}_{dp}]_i + \max_{\boldsymbol{\zeta}^{\mathrm{u}}_{dp}\in\Omega^{\mathrm{u}}_{dp}} \left(-\boldsymbol{b}_d^{\top}\boldsymbol{\zeta}^{\mathrm{u1}}_{dp} - \boldsymbol{b}_{dp}^{\top}\boldsymbol{\zeta}^{\mathrm{u2}}_{dp}\right) \geq 0,\\ \forall d\in\mathcal{D}, p\in\boldsymbol{P}_d, i\in\{1,\ldots,\rho_{dp}\},\end{aligned} \tag{A11}$$

where $\boldsymbol{\zeta}^{\mathrm{u}}_{dp} = \{\boldsymbol{\zeta}^{\mathrm{u1}}_{dp}, \boldsymbol{\zeta}^{\mathrm{u2}}_{dp}\}$ and Ω^{u}_{dp} includes $\boldsymbol{\zeta}^{\mathrm{u}}_{dp}\geq 0$ and the following constraints

$$\begin{aligned}A_d^{\top}\boldsymbol{\zeta}^{\mathrm{u1}}_{dp} + B_{dp}^{\top}\boldsymbol{\zeta}^{\mathrm{u2}}_{dp} - [\mathscr{A}_{dp}]_i^{\top} = 0,\\ \forall d\in\mathcal{D}, p\in\boldsymbol{P}_d, i\in\{1,\ldots,\rho_{dp}\}.\end{aligned}$$

Constraints (A11) are further recast as

$$\begin{aligned}&[\bar{\boldsymbol{x}}^{\mathrm{c}}_d]_i - [\boldsymbol{\upsilon}_{dp}]_i - \boldsymbol{b}_d^{\top}\boldsymbol{\zeta}^{\mathrm{u1}}_{dp} - \boldsymbol{b}_{dp}^{\top}\boldsymbol{\zeta}^{\mathrm{u2}}_{dp} \geq 0,\\ &\qquad\forall d\in\mathcal{D}, p\in\boldsymbol{P}_d, i\in\{1,\ldots,\rho_{dp}\},\end{aligned} \tag{A12a}$$

$$\begin{aligned}&A_d^{\top}\boldsymbol{\zeta}^{\mathrm{u1}}_{dp} + B_{dp}^{\top}\boldsymbol{\zeta}^{\mathrm{u2}}_{dp} - [\mathscr{A}_{dp}]_i^{\top} = 0,\\ &\qquad\forall d\in\mathcal{D}, p\in\boldsymbol{P}_d, i\in\{1,\ldots,\rho_{dp}\}.\end{aligned} \tag{A12b}$$

REFERENCES

[1] A. Jenn, "Emissions of electric vehicles in california's transition to carbon neutrality," *Appl. Energy*, vol. 339, p. 120974, 2023.

[2] J. Wang, C. Huang, D. He, and R. Tu, "Range anxiety among battery electric vehicle users: Both distance and waiting time matter," in *Proceedings of the Human Factors and Ergonomics Society Annual Meeting*, vol. 67, no. 1. SAGE Publications Sage CA: Los Angeles, CA, 2023, pp. 1309–1315.

[3] C. Yao, S. Chen, M. Salazar, and Z. Yang, "Joint routing and charging problem of electric vehicles with incentive-aware customers considering spatio-temporal charging prices," *IEEE Trans. Intell. Transp. Syst.*, vol. 24, no. 11, pp. 12 215–12 226, 2023.

[4] H. Zhang, S. J. Moura, Z. Hu, W. Qi, and Y. Song, "A second-order cone programming model for planning pev fast-charging stations," *IEEE Trans. Power Syst.*, vol. 33, no. 3, pp. 2763–2777, 2018.

[5] Y. Deng, Y. Zhang, F. Luo, and Y. Mu, "Operational planning of centralized charging stations utilizing second-life battery energy storage systems," *IEEE Trans. Sustain. Energy.*, vol. 12, no. 1, pp. 387–399, 2021.

[6] C. Yao, S. Chen, and Z. Yang, "Cooperative operation of the fleet operator and incentive-aware customers in an on-demand delivery system: A bilevel approach," *IEEE Internet Things J.*, vol. 11, no. 6, pp. 9668–9680, 2024.

[7] F. Xia, H. Chen, M. Shahidehpour, W. Gan, M. Yan, and L. Chen, "Distributed expansion planning of electric vehicle dynamic wireless charging system in coupled power-traffic networks," *IEEE Trans. Smart Grid*, vol. 12, no. 4, pp. 3326–3338, 2021.

[8] V. Z. Barsari, D. J. Thrimawithana, and G. A. Covic, "An inductive coupler array for in-motion wireless charging of electric vehicles," *IEEE Trans. Power Electron.*, vol. 36, no. 9, pp. 9854–9863, 2021.

[9] M. Paris, "Wireless charging: The roads where electric vehicles never need to plug in," January 2024, [Online]. Available: www.bbc.com/future/article/20240130-wireless-charging-the-roads-where-electric-vehicles-\never-need-to-plug-in.

[10] F. Paparella, T. Hofman, and M. Salazar, "Cost-optimal fleet management strategies for solar-electric autonomous mobility-on-demand systems," in *2023 IEEE 26th International Conference on Intelligent Transportation Systems (ITSC)*. IEEE, 2023, pp. 5410–5415.

[11] F. Xia, H. Chen, M. Yan, W. Gan, Q. Zhou, T. Ding, X. Wang, L. Wang, and L. Chen, "Market-based coordinated planning of fast charging station and dynamic wireless charging system considering energy demand assignment," *IEEE Trans. Smart Grid*, vol. 15, no. 2, pp. 1913–1925, 2024.

[12] W. Liu, Q. Wang, and Y. Xu, "Traffic toll design for dynamic wireless charging in coupled power-transportation networks: A tri-level optimization approach," *IEEE Trans. Smart Grid*, vol. 15, no. 5, pp. 4877–4889, 2024.

[13] S. D. Manshadi, M. E. Khodayar, K. Abdelghany, and H. Üster, "Wireless charging of electric vehicles in electricity and transportation networks," *IEEE Trans. Smart Grid*, vol. 9, no. 5, pp. 4503–4512, 2018.

[14] J. He, H. Yang, T.-Q. Tang, and H.-J. Huang, "Optimal deployment of wireless charging lanes considering their adverse effect on road capacity," *Transp. Res. Part C: Emerg. Technol.*, vol. 111, pp. 171–184, 2020.

[15] C. Q. Tran, M. Keyvan-Ekbatani, D. Ngoduy, and D. Watling, "Dynamic wireless charging lanes location model in urban networks considering route choices," *Transp. Res. Part C: Emerg. Technol.*, vol. 139, p. 103652, 2022.

[16] M. He, S. Wang, and C. Zhuge, "A data-driven large-scale microsimulation approach to deploying and operating wireless charging lanes," *Transp. Res. Part D: Transp. Environ.*, vol. 121, p. 103835, 2023.

[17] W. Liu, X. Wang, and Y. Xu, "Bilevel planning of wireless charging lanes in coupled transportation and power distribution networks," *IEEE Trans. Transp. Electrif.*, vol. 10, no. 2, pp. 2499–2510, 2023.

[18] I. Hwang, Y. J. Jang, Y. D. Ko, and M. S. Lee, "System optimization for dynamic wireless charging electric vehicles operating in a multiple-route environment," *IEEE Trans. Intell. Transp. Syst.*, vol. 19, no. 6, pp. 1709–1726, 2017.

[19] Y. Tao, J. Qiu, S. Lai, G. Wang, H. Liu, and X. Sun, "Coordinated planning of dynamic wireless charging systems and electricity networks considering range anxiety of electric vehicles," *IEEE Trans. Smart Grid*, 2024.

[20] M. Pei, H. Zhu, J. Ling, Y. Hu, H. Yao, and L. Zhong, "Empowering highway network: Optimal deployment and strategy for dynamic wireless charging lanes," *Commun. Transp. Res.*, vol. 3, p. 100106, 2023.

[21] W. Li, Y. He, S. Hu, Z. He, and C. Ratti, "Planning dynamic wireless charging infrastructure for battery electric bus systems with the joint optimization of charging scheduling," *Transp. Res. Part C: Emerg. Technol.*, vol. 159, p. 104469, 2024.

[22] S. Liu, D. Z. Wang, Q. Tian, and Y. H. Lin, "Optimal configuration of dynamic wireless charging facilities considering electric vehicle battery capacity," *Transp. Res. Part E: Logist. Transp. Rev.*, vol. 181, p. 103376, 2024.

[23] R. Chen, X. Qian, L. Miao, and S. V. Ukkusuri, "Optimal charging facility location and capacity for electric vehicles considering route choice and charging time equilibrium," *Comput. Oper. Res.*, vol. 113, p. 104776, 2020.

[24] J. Ji, L. Wang, M. Yang, Y. Bie, and M. Hao, "Optimal deployment of dynamic wireless charging facilities for electric bus route considering stochastic travel times," *Energy*, vol. 289, p. 129873, 2024.

[25] Z. Liu and Z. Song, "Robust planning of dynamic wireless charging infrastructure for battery electric buses," *Transp. Res. Part C: Emerg. Technol.*, vol. 83, pp. 77–103, 2017.

[26] Y. Alwesabi, F. Avishan, İ. Yanıkoğlu, Z. Liu, and Y. Wang, "Robust strategic planning of dynamic wireless charging infrastructure for electric buses," *Appl. Energy*, vol. 307, p. 118243, 2022.

[27] Y. Wang, Y. Zhou, and X. Yan, "Reliable dynamic wireless charging infrastructure deployment problem for public transport services," *Euro. J. Oper. Res.*, vol. 313, no. 2, pp. 747–766, 2024.

[28] L. Jiang, Y. Hua, C. Ma, and X. Liu, "Sunchase: Energy-efficient route planning for solar-powered EVs," in *2017 IEEE 37th International Conference on Distributed Computing Systems (ICDCS)*. IEEE, 2017, pp. 383–393.

[29] P. Zhou, C. Wang, and Y. Yang, "Design and optimization of solar-powered shared electric autonomous vehicle system for smart cities," *IEEE Trans. Mobile Comput.*, vol. 22, no. 4, pp. 2053–2068, 2021.

[30] C. Yao, S. Chen, and Z. Yang, "Online distributed routing problem of electric vehicles," *IEEE Trans. Intell. Transp. Syst.*, vol. 23, no. 9, pp. 16 330–16 341, 2022.

[31] S. Jiang, J. Cheng, K. Pan, F. Qiu, and B. Yang, "Data-driven chance-constrained planning for distributed generation: A partial sampling approach," *IEEE Trans. Power Syst.*, vol. 38, no. 6, pp. 5228–5244, 2022.

[32] E. Delage and Y. Ye, "Distributionally robust optimization under moment uncertainty with application to data-driven problems," *Oper. Res.*, vol. 58, no. 3, pp. 595–612, 2010.

[33] M. Cheramin, J. Cheng, R. Jiang, and K. Pan, "Computationally efficient approximations for distributionally robust optimization under moment and Wasserstein ambiguity," *INFORMS J. Comput.*, vol. 34, no. 3, pp. 1768–1794, 2022.

[34] A. M. Fathabad, J. Cheng, K. Pan, and F. Qiu, "Data-driven planning for renewable distributed generation integration," *IEEE Trans. Power Syst.*, vol. 35, no. 6, pp. 4357–4368, 2020.

[35] G. A. Hanasusanto, D. Kuhn, and W. Wiesemann, "K-adaptability in two-stage robust binary programming," *Oper. Res.*, vol. 63, no. 4, pp. 877–891, 2015.

[36] D. Kuhn, W. Wiesemann, and A. Georghiou, "Primal and dual linear decision rules in stochastic and robust optimization," *Math. Program.*, vol. 130, pp. 177–209, 2011.

[37] A. Subramanyam, C. E. Gounaris, and W. Wiesemann, "K-adaptability in two-stage mixed-integer robust optimization," *Math. Program. Comput.*, vol. 12, no. 2, pp. 193–224, 2020.

[38] A. Ben-Tal, "Robust optimization," *Princeton University Press*, vol. 2, pp. 35–53, 2009.

[39] G. Angulo, S. Ahmed, and S. S. Dey, "Improving the integer L-shaped method," *INFORMS J. Comput.*, vol. 28, no. 3, pp. 483–499, 2016.

[40] R. Rahmaniani, S. Ahmed, T. G. Crainic, M. Gendreau, and W. Rei, "The benders dual decomposition method," *Oper. Res.*, vol. 68, no. 3, pp. 878–895, 2020.

[41] S. Boyd, L. Xiao, and A. Mutapcic, "Subgradient methods," *Lecture notes of EE392o, Stanford University, Autumn Quarter*, vol. 2004, no. 01, 2003.

[42] R. Tribdino, "Scania tests its first solar-powered trucks, sees the technology to grow," 2024. [Online]. Available: https://cleantechnica.com/2023/08/31/scania-tests-its-first-solar-powered-trucks-sees-the-technology-to-grow/

[43] L. Xue, V. Galigekere, G.-j. Su, R. Zeng, M. Mohammad, E. Gurpinar, S. Chowdhury, and O. Onar, "Design and analysis of a 200 kW dynamic wireless charging system for electric vehicles," in *2022 IEEE Applied Power Electronics Conference and Exposition (APEC)*, 2022, pp. 1096–1103.

[44] J. Zhang, Z. Wang, P. Liu, and Z. Zhang, "Energy consumption analysis and prediction of electric vehicles based on real-world driving data," *Appl. Energy*, vol. 275, p. 115408, 2020.

[45] Z. Bi, G. A. Keoleian, Z. Lin, M. R. Moore, K. Chen, L. Song, and Z. Zhao, "Life cycle assessment and tempo-spatial optimization of deploying dynamic wireless charging technology for electric cars," *Transp. Res. Part C: Emerg. Technol.*, vol. 100, pp. 53–67, 2019.

[46] M. Šúri, T. A. Huld, and E. D. Dunlop, "PV-GIS: a web-based solar radiation database for the calculation of PV potential in Europe," *Int. J. Sustain. Energy*, vol. 24, no. 2, pp. 55–67, 2005.